

1 Quasi-consistent efficient meshfree thin shell
2 formulation ~~to-with~~ naturally ~~aaccommodate stabilized~~
3 ~~enforced~~ essential boundary conditions

4 Junchao Wu^{a,*}, Yangtao Xu^a, Bin Xu^a, Syed Humayun Basha^a

^a*Key Laboratory for Intelligent Infrastructure and Monitoring of Fujian Province, Key Laboratory for Structural Engineering and Disaster Prevention of Fujian Province, College of Civil Engineering, Huaqiao University, Xiamen, Fujian, 361021, China*

5 **Abstract**

This research proposed an ~~eficient efficient~~ and quasi-consistent meshfree thin shell formulation with ~~natural naturally stabilized~~ enforcement of essential boundary conditions. Within the framework of the Hu-Washizu variational principle, a mixed formulation of displacements, strains and stresses is employed in this approach, where the displacements are discretized using meshfree shape functions, and the strains and stresses are expressed using smoothed gradients, ~~covariant smoothed gradients~~ and covariant bases. The smoothed gradients satisfy the first ~~and second order second-order~~ integration constraint and ~~have quasi-consistent consistency observed variational consistency for polynomial strains and stresses~~. Owing to Hu-Washizu variational principle, the essential boundary conditions automatically arise in its weak form. As a result, the suggested technique's enforcement of essential boundary conditions resembles that of the traditional Nitsche's method. Contrary to Nitsche's method, the costly higher order derivatives of conventional meshfree shape functions ~~were are~~ replaced by the smoothed gradients with fast computation, which improve the efficiency. Meanwhile, the proposed formulation features a naturally stabilized term without adding any artificial stabilization factors, which eliminates the ~~stabilization parameter-dependent issue in the Nitsche's method . The application of penalty method as a stabilization. Further, the~~ efficacy of the proposed Hu-Washizu meshfree thin shell formulation is illustrated by a set of classical standard thin shell problems.

6 *Keywords:* Meshfree, Thin shell, Hu-Washizu variational principle,
7 Reproducing kernel gradient smoothing, Essential boundary condition

*Corresponding author
Email address: jcwu@hqu.edu.cn (Junchao Wu)

8 1. Introduction

9 Thin shell structures generally adhere to the Kirchhoff hypothesis [1], that
10 neglects the shear deformation can be described using Galerkin formulation
11 which requires to have at least C^1 continuity. The traditional finite element
12 methods usually ~~only~~ have C^0 continuous shape functions, and it prefers Mindlin
13 thick shear theory, hybrid and mixed models in simulation of shell structure [2].
14 Meshfree methods [3, 4, 5] with high order smoothed shape functions have gar-
15 nered much research attention over the past thirty years. These techniques
16 established the shape functions based on a collection of dispersed nodes, and
17 the high order continuity of shape functions can be easily achieved even with
18 low-order basis functions. For thin shell analysis, ~~this~~-high order meshfree ap-
19 proximation can also ~~further~~ alleviate the membrane locking caused by the
20 mismatched approximation order of membrane strain and bending strain [6].
21 Furthermore~~Moreover~~, nodal-based meshfree approximations generally offer the
22 flexibility of local refinement and can relieve the burden of mesh distortion.
23 Owing to these benefits, numerous meshfree techniques have been developed
24 and implemented in many scientific and engineering fields ~~[7, 8, 9, 10, 11, 12]~~
25 ~~[7, 8, 9, 10, 11, 12, 13]~~. However, the high order smoothed meshfree shape func-
26 tions accompany the enlarged and overlapping supports, which may potentially
27 cause many problems for shape functions. One of the issues is the loss of the
28 Kronecker delta property, which means that, unlike the finite element methods,
29 the necessary boundary conditions cannot be directly enforced [14]. Another
30 issue is that the variational consistency or said integration constraint, ~~which~~
31 ~~is a condition that requires the formulation to exactly reproduce the solution~~
32 ~~spanned by the basis functions~~, cannot be satisfied~~due to~~. This issue is mainly
33 caused by the misalignment between the numerical integration domains and sup-
34 ports of shape functions. ~~Besides~~~~Thus~~, the shape functions exhibit a piecewise
35 rational nature in each integration domain. ~~Besides, it has to be noted that the~~
36 ~~traditional integration rules like Gauss scheme cannot ensure the integration~~
37 ~~accuracy in Galerkin weak form [15, 16]~~. Therefore, variational consistency
38 is vital to the solution accuracy in ~~Galerkin formulations [15, 16]~~
39 ~~the Galerkin meshfree formulations~~.

40 Various ways have been presented to enforce the necessary boundary for
41 Galerkin meshfree methods directly, including the boundary singular kernel
42 method [17], mixed transformation method [17], and interpolation element-free
43 method [18] for recovering shape functions' Kronecker property. However, these
44 methods ~~are~~
~~were~~ not based on a variational setting and cannot guarantee vari-
45 ational consistency. In the absence of a meshfree node, accuracy enforcement
46 might be ~~poorer~~
~~poor~~. In contrast, enforcing the essential boundary conditions
47 using a variational approach is preferred for Galerkin meshfree methods. The
48 variational consistent Lagrange multiplier approach was initially used to the
49 Galerkin meshfree method by Belytschko et al. [3]. In this method, the extra
50 degrees of freedom are used to determine the discretion of Lagrange multiplier.
51 Furthermore, Ivannikov et al. [19] ~~have~~ extended this approach to geometri-
52 cally nonlinear thin shells. Lu et al. [20] suggested the modified variational es-

53 sential boundary enforcement approach and expressed the Lagrange multiplier
54 by equivalent tractions to eliminate the excess degrees of freedom. However,
55 the coercivity of this approach is not always ensured and potentially reduces
56 the accuracy. Zhu and Atluri [21] pioneered the penalty method for meshfree
57 method, making it a straightforward approach to enforce essential boundary
58 conditions via Galerkin weak form. However, the penalty method lacks varia-
59 tional consistency and requires experimental artificial parameters whose optimal
60 value is hard to determine. Fernández-Méndez and Huerta [14] imposed neces-
61 sary boundary conditions using Nitsche's approach in the meshfree formulation.
62 This approach can be seen as a hybrid combination of the modified variational
63 method and the penalty method because the modified variational method gen-
64 erates variational consistency through the use of a consistent term, and the
65 penalty method is used as a stabilized term to recover the coercivity. Skatulla
66 and Sansour [22] extended Nitsche's thin shell analysis method and proposed an
67 iteration algorithm to determine artificial parameters at each integration point.

68 In order to address the issue of numerical integration, a series of consis-
69 tent integration schemes have been developed for Galerkin meshfree methods.
70 Among these include stabilized conforming nodal integration [23], variational
71 consistent integration [24], quadratic consistent integration [25], reproducing
72 kernel gradient smoothing integration [26], and consistent projection integration
73 [27]. The assumed strain approach establishes the most consistent integration
74 scheme, while the smoothed gradient replaces the costly higher order derivatives
75 of traditional meshfree shape functions and shows a high efficiency. Moreover, to
76 achieve global variational consistency, a consistent essential boundary condition
77 enforcement ~~should cooperate must be combined~~ with the consistent integra-
78 tion scheme. The ~~combination of~~ consistent integration scheme and Nitsche's
79 method for treating essential boundary conditions ~~show a good performance~~
80 ~~since they may demonstrate better performance since both the methods~~ can
81 satisfy the coercivity without requiring additional degrees of freedom. Never-
82 theless, Nitsche's approach still retains the artificial parameters in ~~the~~ stabilized
83 terms, and it is essential to remain ~~conscious cautious~~ of the costly higher order
84 derivatives, particularly for thin plate and thin shell problems. Recently, Wu
85 et al. [28, 29] proposed an efficient and stabilized essential boundary condition
86 enforcement method based upon the Hellinger-Reissner variational principle,
87 where a mixed formulation in Hellinger-Reissner weak form recasts the repro-
88 ducing kernel gradient smoothing integration. The terms ~~required~~ for enforcing
89 essential boundary conditions are identical to the Nitsche's method, and both
90 have consistent and stabilized terms. ~~Nevertheless~~
~~However~~, the stabilized term
91 of this method naturally exists in the Hellinger-Reissner weak form and no longer
92 needs the artificial parameters, even for essential boundary enforcement; ~~instead~~
93 ~~. Instead~~ all of the higher order derivatives are represented by ~~the~~ smoothed
94 gradients and their derivatives.

95 In this study, an efficient and stabilized variational consistent meshfree
96 method that naturally enforces the essential boundary conditions is developed
97 for thin shell ~~structure~~
~~structures~~. Following the concept of the Hellinger-Reissner
98 principle base consistent meshfree method, the Hu-Washizu variational prin-

99 ciple of complementary energy with variables of displacement, strains, and
100 stresses ~~is-were~~ employed. The displacement is approximated by conventional
101 meshfree shape functions, and the strains and stresses ~~are-were~~ expressed by
102 smoothed gradients with covariant bases. It is important to note that al-
103 though the first second-order integration requirements ~~are-were~~ naturally em-
104 bedded in the smoothed gradients, their fulfillment ~~can-only result resulted~~ in
105 a quasi-satisfaction of variational consistency. ~~This is mainly~~ because of the
106 non-polynomial nature of the stresses. Hu-Washizu's weak form ~~is-was~~ used
107 to evaluate all the essential boundary conditions regarding displacements and
108 rotations. This type of formulation is similar to the Nitsche's method but does
109 not require any artificial parameters. Compared with Nitsche's method, con-
110 ventional reproducing smoothed gradients and its direct derivatives replace the
111 costly higher order derivatives. By utilizing the advantages of a replicating
112 kernel gradient smoothing framework, the smoothed gradients showed better
113 performance compared to conventional derivatives of shape functions, hence
114 increasing the meshfree formulation's computational efficiency.

115 The remainder of this research ~~paper article~~ is structured as follows: The
116 kinematics of the thin shell structure and the weak form of the associated Hu-
117 Washizu principle are briefly described in Section 2. ~~Subsequently, the The~~
118 mixed formulation regarding the displacements, strains and stresses in accor-
119 dance with Hu-Washizu weak form are presented in Section 3. The discrete
120 equilibrium equations are derived in Section 4 using the naturally occurring
121 accommodation of essential, ~~and~~. ~~Subsequently,~~ they are compared to the
122 equations obtained using Nitsche's method. The numerical results in Section 5
123 validate the efficacy of the proposed Hu-Washizu meshfree thin shell formula-
124 tion. Lastly, the concluding remarks are presented in Section 6.

¹²⁵ **2. Hu-Washizu's formulation of complementary energy for thin shell**

¹²⁶ *2.1. Kinematics for thin shell*

¹²⁷ Consider the configuration of a shell $\bar{\Omega}$, as shown in Fig. 1, which can be
¹²⁸ easily described by a parametric curvilinear coordinate system $\xi = \{\xi^i\}_{i=1,2,3}$.
¹²⁹ The mid-surface of the shell denoted by Ω is specified by the in-plane coordinates
¹³⁰ $\xi = \{\xi^\alpha\}_{\alpha=1,2}$, as the thickness direction of shell is by ξ^3 , $-\frac{h}{2} \leq \xi^3 \leq \frac{h}{2}$, h is
¹³¹ the thickness of shell. In this work, Latin indices take the values from 1 to 3,
¹³² and Greek indices are evaluated by 1 or 2. For the Kirchhoff hypothesis [6], the
¹³³ position $\mathbf{x} \in \bar{\Omega}$ is defined by linear functions with respect to ξ^3 :

$$\mathbf{x}(\xi^1, \xi^2, \xi^3) = \mathbf{r}(\xi^1, \xi^2) + \xi^3 \mathbf{a}_3(\xi^1, \xi^2) \quad (1)$$

in which \mathbf{r} means the position on the mid-surface of shell, and \mathbf{a}_3 is correspond-

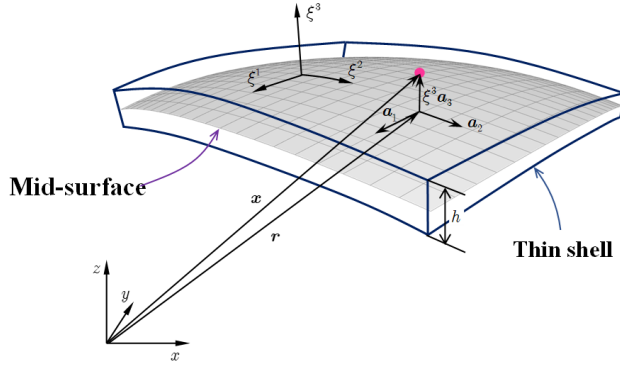


Figure 1: Kinematics for thin shell.

¹³⁴
¹³⁵ ing normal direction. For the mid-surface of shell, the in-plane covariant base
¹³⁶ vector with respect to ξ^α can be derived by a trivial partial differentiation to \mathbf{r} :

$$\mathbf{a}_\alpha = \frac{\partial \mathbf{r}}{\partial \xi^\alpha} = \mathbf{r}_{,\alpha}, \alpha = 1, 2 \quad (2)$$

¹³⁷ to provide for a clear expression, the subscript comma denotes the partial dif-
¹³⁸ ferentiation operation with respect to in-plane coordinates ξ^α , and the normal
¹³⁹ vector \mathbf{a}_3 can be obtained by the normalized cross product of \mathbf{a}_α 's as follows:

$$\mathbf{a}_3 = \frac{\mathbf{a}_1 \times \mathbf{a}_2}{\|\mathbf{a}_1 \times \mathbf{a}_2\|} \quad (3)$$

¹⁴⁰ where $\|\bullet\|$ is the Euclidean norm operator.

¹⁴¹ With the assumption of infinitesimal deformation, the strain components
¹⁴² with respect to the global contravariant base can be stated as:

$$\epsilon_{ij} = \frac{1}{2} (\mathbf{x}_{,i} \cdot \mathbf{u}_{,j} + \mathbf{u}_{,i} \cdot \mathbf{x}_{,j}) \quad (4)$$

¹⁴³ where \mathbf{u} represents the displacement for the shell deformation. To satisfy the
¹⁴⁴ Kirchhoff hypothesis, the displacement is assumed to be of the following form:

$$\mathbf{u}(\xi^1, \xi^2, \xi^3) = \mathbf{v}(\xi^1, \xi^2) + \boldsymbol{\theta}(\xi^1, \xi^2)\xi^3 \quad (5)$$

¹⁴⁵ in which the quadratic and higher order terms are neglected. $\mathbf{v}, \boldsymbol{\theta}$ represent
¹⁴⁶ the displacement and rotation in mid-surface, respectively.

¹⁴⁷ Subsequently, plugging Eqs. (1) and (5) into Eq. (4) and neglecting the
¹⁴⁸ quadratic terms, the strain components can be rephrased as follows:

$$\begin{aligned} \epsilon_{\alpha\beta} &= \frac{1}{2}(\mathbf{a}_\alpha \cdot \mathbf{v}_{,\beta} + \mathbf{v}_{,\alpha} \cdot \mathbf{a}_\beta) \\ &+ \frac{1}{2}(\mathbf{a}_{3,\alpha} \cdot \mathbf{v}_{,\beta} + \mathbf{v}_{,\alpha} \cdot \mathbf{a}_{3,\beta} + \mathbf{a}_\alpha \cdot \boldsymbol{\theta}_{,\beta} + \boldsymbol{\theta}_{,\alpha} \cdot \mathbf{a}_\beta)\xi^3 \end{aligned} \quad (6a)$$

$$\epsilon_{\alpha\beta} = \varepsilon_{\alpha\beta} + \kappa_{\alpha\beta}\xi^3 \quad (6b)$$

$$\epsilon_{\alpha 3} = \frac{1}{2}(\mathbf{a}_\alpha \cdot \boldsymbol{\theta} + \mathbf{v}_{,\alpha} \cdot \mathbf{a}_3) + \frac{1}{2}(\mathbf{a}_3 \cdot \boldsymbol{\theta})_{,\alpha}\xi^3 \quad (6c)$$

¹⁴⁹ where $\varepsilon_{\alpha\beta}, \kappa_{\alpha\beta}$ represent membrane and bending strains, respectively, and are
¹⁵⁰ given as follows:

$$\varepsilon_{\alpha\beta} = \frac{1}{2}(\mathbf{a}_\alpha \cdot \mathbf{v}_{,\beta} + \mathbf{v}_{,\alpha} \cdot \mathbf{a}_\beta) \quad (7)$$

$$\kappa_{\alpha\beta} = \frac{1}{2}(\mathbf{a}_{3,\alpha} \cdot \mathbf{v}_{,\beta} + \mathbf{v}_{,\alpha} \cdot \mathbf{a}_{3,\beta} + \mathbf{a}_\alpha \cdot \boldsymbol{\theta}_{,\beta} + \boldsymbol{\theta}_{,\alpha} \cdot \mathbf{a}_\beta) \quad (8)$$

¹⁵¹ In accordance with the Kirchhoff hypothesis, the thickness of shell will not
¹⁵² change, and the deformation related with direction of ξ^3 will vanish, i.e. $\epsilon_{3i} = 0$.
¹⁵³ Thus, the rotation $\boldsymbol{\theta}$ can be rewritten as:

$$\epsilon_{3i} = 0 \Rightarrow \begin{cases} \boldsymbol{\theta} \cdot \mathbf{a}_\alpha \cancel{=} -\mathbf{v}_{,\alpha} \cdot \mathbf{a}_3 \cancel{=} 0 \\ \boldsymbol{\theta} \cdot \mathbf{a}_3 = 0 \end{cases} \Rightarrow \boldsymbol{\theta} = -\mathbf{v}_{,\alpha} \cdot \mathbf{a}_3 \mathbf{a}^\alpha \quad (9)$$

¹⁵⁵ where \mathbf{a}^α 's is the in-plane contravariant base vector, $\mathbf{a}^\alpha \cdot \mathbf{a}_\beta = \delta_\beta^\alpha$, δ is the
¹⁵⁶ Kronecker delta function. Substituting Eq. 9 into Eq. (8) leads to:
¹⁵⁷ The detailed derivation of Eq. 9 can be found in [31].

¹⁵⁸ Furthermore, on substituting Eq. (9) into Eq. (8) leads to:

$$\kappa_{\alpha\beta} = (\Gamma_{\alpha\beta}^\gamma \mathbf{v}_{,\gamma} - \mathbf{v}_{,\alpha\beta}) \cdot \mathbf{a}_3 = -\mathbf{v}_{,\alpha}|_\beta \cdot \mathbf{a}_3 \quad (10)$$

¹⁵⁹ in which $\Gamma_{\alpha\beta}^\gamma = \mathbf{a}_{\alpha,\beta} \cdot \mathbf{a}^\gamma$ is namely the Christoffel symbol of the second kind, and
¹⁶⁰ $\mathbf{v}_{,\alpha}|_\beta$ is the in-plane covariant derivative of $\mathbf{v}_{,\alpha}$, i.e. $\mathbf{v}_{,\alpha}|_\beta = \Gamma_{\alpha\beta}^\gamma \mathbf{v}_{,\gamma} - \mathbf{v}_{,\alpha\beta}$.

¹⁶¹ 2.2. Galerkin weak form for Hu-Washizu principle of complementary energy

¹⁶² In this study, the Hu-Washizu variational principle of complementary energy
¹⁶³ [32] was adopted for the development of the proposed analytical approach, the

¹⁶⁴ corresponding complementary functional, denoted by Π_C , is listed as follows:

$$\begin{aligned} & \Pi_C(\varepsilon_{\alpha\beta}, \kappa_{\alpha\beta}, N^{\alpha\beta}, M^{\alpha\beta}) \\ &= \int_{\Omega} \frac{h}{2} \varepsilon_{\alpha\beta} C^{\alpha\beta\gamma\eta} \varepsilon_{\gamma\eta} d\Omega + \int_{\Omega} \frac{h^3}{24} \kappa_{\alpha\beta} C^{\alpha\beta\gamma\eta} \kappa_{\gamma\eta} d\Omega \\ &+ \int_{\Omega} \varepsilon_{\alpha\beta} (N^{\alpha\beta} - h C^{\alpha\beta\gamma\eta} \varepsilon_{\gamma\eta}) d\Omega + \int_{\Omega} \kappa_{\alpha\beta} (M^{\alpha\beta} - \frac{h^3}{12} C^{\alpha\beta\gamma\eta} \kappa_{\gamma\eta}) d\Omega \\ &- \int_{\Gamma_v} \mathbf{T} \cdot \bar{\mathbf{v}} d\Gamma + \int_{\Gamma_\theta} M_{\mathbf{n}\mathbf{n}} \bar{\theta}_{\mathbf{n}} d\Gamma - (P \mathbf{a}_3 \cdot \bar{\mathbf{v}})_{\mathbf{x} \in C_w} \end{aligned} \quad (11)$$

¹⁶⁵ where $C^{\alpha\beta\gamma\eta}$'s represent the components of fourth order elasticity tensor with
¹⁶⁶ respect to the covariant base and plane stress assumption, and it can be ex-
¹⁶⁷ pressed by Young's modulus E , Poisson's ratio ν and the in-plane contravariant
¹⁶⁸ metric coefficients $a^{\alpha\beta}$'s, $a^{\alpha\beta} = \mathbf{a}^\alpha \cdot \mathbf{a}^\beta$, as follows:

$$C^{\alpha\beta\gamma\eta} = \frac{E}{2(1+\nu)} (a^{\alpha\gamma} a^{\beta\eta} + a^{\alpha\eta} a^{\beta\gamma} + \frac{2\nu}{1-\nu} a^{\alpha\beta} a^{\gamma\eta}) \quad (12)$$

¹⁶⁹ and $N^{\alpha\beta}$, $M^{\alpha\beta}$ ~~are represent~~ the components of ~~membrane and bending stresses~~
¹⁷⁰ ~~membrane- and bending- stresses which are~~ given by:

$$N^{\alpha\beta} = h C^{\alpha\beta\gamma\eta} \varepsilon_{\gamma\eta}, \quad M^{\alpha\beta} = \frac{h^3}{12} C^{\alpha\beta\gamma\eta} \kappa_{\gamma\eta} \quad (13)$$

¹⁷¹ Essential boundaries on the edges and corners denoted by Γ_v , Γ_θ and C_v
¹⁷² are naturally existed in complementary energy functional, ~~and~~ $\bar{\mathbf{v}}$, $\bar{\theta}_{\mathbf{n}}$ are the
¹⁷³ corresponding prescribed displacement and normal rotation, respectively. \mathbf{T} ,
¹⁷⁴ $M_{\mathbf{n}\mathbf{n}}$ and P can be determined by Euler-Lagrange equations of shell problem
¹⁷⁵ [31] as follows:

$$\mathbf{T} = \mathbf{T}_N + \mathbf{T}_M \rightarrow \begin{cases} \mathbf{T}_N = \mathbf{a}_\alpha N^{\alpha\beta} n_\beta \\ \mathbf{T}_M = (\mathbf{a}_3 M^{\alpha\beta} s_\alpha n_\beta)_{,\gamma} s^\gamma + (\mathbf{a}_3 M^{\alpha\beta})|_\beta n_\alpha \end{cases} \quad (14)$$

¹⁷⁶ $M_{\mathbf{n}\mathbf{n}} = M^{\alpha\beta} n_\alpha n_\beta \quad (15)$

¹⁷⁷ $P = -[[M^{\alpha\beta} s_\alpha n_\beta]] \quad (16)$

¹⁷⁸ where $\mathbf{n} = n^\alpha \mathbf{a}_\alpha = n_\alpha \mathbf{a}^\alpha$ and $\mathbf{s} = s^\alpha \mathbf{a}_\alpha = s_\alpha \mathbf{a}^\alpha$ are the outward normal and
¹⁷⁹ tangent directions on boundaries. $[[f]]$ is the jump operator defined by:

$$[[f]]_{\mathbf{x}=\mathbf{x}_c} = \lim_{\epsilon \rightarrow 0^+} (f(\mathbf{x}_c + \epsilon) - f(\mathbf{x}_c - \epsilon)), \mathbf{x}_c \in \Gamma \quad (17)$$

¹⁸⁰ where f is an arbitrary function on Γ .

¹⁸¹ Moreover, the natural boundary conditions should be applied by Lagrangian
¹⁸² multiplier method with displacement \mathbf{v} regarded as multiplier. Thus, then the

¹⁸³ new complementary energy functional namely Π is given by:

$$\begin{aligned} & \Pi(\mathbf{v}, \varepsilon_{\alpha\beta}, \kappa_{\alpha\beta}, N^{\alpha\beta}, M^{\alpha\beta}) \\ &= \Pi_C(\varepsilon_{\alpha\beta}, \kappa_{\alpha\beta}, N^{\alpha\beta}, M^{\alpha\beta}) + \int_{\Gamma_M} \theta_n (M_{nn} - \bar{M}_{nn}) d\Gamma \\ & \quad - \int_{\Gamma_T} \mathbf{v} \cdot (\bar{\mathbf{T}}) d\Gamma - \mathbf{v} \cdot \mathbf{a}_3 (P - \bar{P})_{x \in C_P} - \int_{\Omega} \mathbf{v} \cdot (\bar{\mathbf{b}}) d\Omega \end{aligned} \quad (18)$$

¹⁸⁴ where $\bar{\mathbf{T}}$, \bar{M}_{nn} and \bar{P} are the prescribed traction, bending moment and
¹⁸⁵ concentrated force on edges Γ_T , Γ_M and corner C_P respectively. All the specified
¹⁸⁶ boundaries meet the following geometric relationships:

$$\begin{cases} \Gamma = \Gamma_v \cup \Gamma_T \cup \Gamma_\theta \cup \Gamma_M, & C = C_v \cup C_P, \\ \Gamma_v \cap \Gamma_T = \Gamma_\theta \cap \Gamma_M = C_v \cap C_P = \emptyset \end{cases} \quad (19)$$

¹⁸⁷ and $\bar{\mathbf{b}}$ stands for the prescribed body force in Ω , \mathbf{b} ~~also~~ can be written based on
¹⁸⁸ Euler-Lagrange equations [31] as:

$$\mathbf{b} = \mathbf{b}_N + \mathbf{b}_M \rightarrow \begin{cases} \mathbf{b}_N = (\mathbf{a}_\alpha N^{\alpha\beta})|_\beta \\ \mathbf{b}_M = (\mathbf{a}_3 M^{\alpha\beta})|_{\alpha\beta} \end{cases} \quad (20)$$

¹⁸⁹ Introducing a standard variational argument to Eq. (18), $\delta\Pi = 0$, and
¹⁹⁰ considering the arbitrariness of virtual variables, $\delta\mathbf{v}$, $\delta\varepsilon_{\alpha\beta}$, $\delta\kappa_{\alpha\beta}$, $N^{\alpha\beta}$, $M^{\alpha\beta}$
¹⁹¹ lead to the following weak form:

$$-\int_{\Omega} h \delta\varepsilon_{\alpha\beta} C^{\alpha\beta\gamma\eta} \varepsilon_{\gamma\eta} d\Omega + \int_{\Omega} \delta\varepsilon_{\alpha\beta} N^{\alpha\beta} d\Omega = 0 \quad (21a)$$

$$-\int_{\Omega} \frac{h^3}{12} \delta\kappa_{\alpha\beta} C^{\alpha\beta\gamma\eta} \kappa_{\gamma\eta} d\Omega + \int_{\Omega} \delta\kappa_{\alpha\beta} M^{\alpha\beta} d\Omega = 0 \quad (21b)$$

$$\begin{aligned} \int_{\Omega} \delta N^{\alpha\beta} \varepsilon_{\alpha\beta} d\Omega - \int_{\Gamma} \delta \mathbf{T}_N \cdot \mathbf{v} d\Gamma + \int_{\Omega} \delta \mathbf{b}_N \cdot \mathbf{v} d\Omega \\ + \int_{\Gamma_v} \delta \mathbf{T}_N \cdot \mathbf{v} d\Gamma = \int_{\Gamma_v} \delta \mathbf{T}_N \cdot \bar{\mathbf{v}} d\Gamma \end{aligned} \quad (21c)$$

¹⁹⁴

$$\begin{aligned} \int_{\Omega} \delta M^{\alpha\beta} \kappa_{\alpha\beta} d\Omega - \int_{\Gamma} \delta M_{nn} \theta_n d\Gamma + \int_{\Gamma} \delta \mathbf{T}_M \cdot \mathbf{v} d\Gamma + (\delta P \mathbf{a}_3 \cdot \mathbf{v})_{x \in C} + \int_{\Omega} \delta \mathbf{b}_M \cdot \mathbf{v} d\Omega \\ + \int_{\Gamma_\theta} \delta M_{nn} \theta_n d\Gamma - \int_{\Gamma_v} \delta \mathbf{T}_M \cdot \mathbf{v} d\Gamma - (\delta P \mathbf{a}_3 \cdot \mathbf{v})_{x \in C_v} \\ = \int_{\Gamma_\theta} \delta M_{nn} \bar{\theta}_n d\Gamma - \int_{\Gamma_v} \delta \mathbf{T}_M \cdot \bar{\mathbf{v}} d\Gamma - (\delta P \mathbf{a}_3 \cdot \bar{\mathbf{v}})_{x \in C_v} \end{aligned} \quad (21d)$$

¹⁹⁵

$$\begin{aligned}
& \int_{\Gamma} \delta \theta_n M_{nn} d\Gamma - \int_{\Gamma} \delta \mathbf{v} \cdot \mathbf{T} d\Gamma - (\delta \mathbf{v} \cdot \mathbf{a}_3 P)_{x \in C} + \int_{\Omega} \delta \mathbf{v} \cdot \mathbf{b} d\Omega \\
& - \int_{\Gamma_\theta} \delta \theta_n M_{nn} d\Gamma + \int_{\Gamma_v} \delta \mathbf{v} \cdot \mathbf{T} d\Gamma + (\delta \mathbf{v} \cdot \mathbf{a}_3 P)_{x \in C_v} = - \int_{\Gamma_T} \delta \mathbf{v} \cdot \bar{\mathbf{t}} d\Gamma - \int_{\Omega} \delta \mathbf{v} \cdot \bar{\mathbf{b}} d\Omega
\end{aligned} \tag{21e}$$

¹⁹⁶ where the geometric relationships of Eq. (19) is used herein.

197 **3. Mixed meshfree formulation for modified Hellinger-Reissner-Hu-Washizu's
198 weak form**

199 *3.1. Reproducing kernel approximation for displacement*

200 This study approximates the displacement by adopting reproducing kernel
201 approximation. As shown in Fig. 2, the mid-surface of the shell Ω is discretized
202 by a set of meshfree nodes $\{\xi_I\}_{I=1}^{n_p}$ in parametric configuration, where n_p is the
203 total number of meshfree nodes. The approximated displacement namely \mathbf{v}^h
204 can be expressed as:

$$\mathbf{v}(\xi) = \sum_{I=1}^{n_p} \Psi_I(\xi) \mathbf{d}_I \quad (22)$$

205 ~~in which where~~ Ψ_I and \mathbf{d}_I ~~is represent~~ the shape function and nodal coefficient
206 tensor related by node ξ_I . According to reproducing kernel approximation [4],
207 the shape function takes the following form:

$$\Psi_I(\xi) = \mathbf{p}^T(\xi) \mathbf{c}(\xi) \phi(\xi_I - \xi) \quad (23)$$

208 where \mathbf{p} is the basis function vector represented using the following quadratic
209 function as:

$$\mathbf{p} = \{1, \xi^1, \xi^2, (\xi^1)^2, \xi^1 \xi^2, (\xi^2)^2\}^T \quad (24)$$

210 The kernel function denoted by ϕ controls the support and smoothness of
211 meshfree shape functions. The quintic B-spline function with square support is
212 used herein as the kernel function:

$$\phi(\xi_I - \xi) = \phi(\hat{s}_1)\phi(\hat{s}_2), \quad \hat{s}_\alpha = \frac{|\xi_I^\alpha - \xi^\alpha|}{s_{\alpha I}} \quad (25)$$

213 with

$$\phi(\hat{s}_\alpha) = \frac{1}{5!} \begin{cases} (3 - 3\hat{s}_\alpha)^5 - 6(2 - 3\hat{s}_\alpha)^5 + 15(1 - 3\hat{s}_\alpha)^5 & \hat{s}_\alpha \leq \frac{1}{3} \\ (3 - 3\hat{s}_\alpha)^5 - 6(2 - 3\hat{s}_\alpha)^5 & \frac{1}{3} < \hat{s}_\alpha \leq \frac{2}{3} \\ (3 - 3\hat{s}_\alpha)^5 & \frac{2}{3} < \hat{s}_\alpha \leq 1 \\ 0 & \hat{s}_\alpha > 1 \end{cases} \quad (26)$$

214 and ~~$\hat{s}_{\alpha I}$ means the characterized size of support for $s_{\alpha I}$ means the support size~~
215 ~~of~~ meshfree shape function Ψ_I .

216 The unknown vector \mathbf{c} in shape function are determined by the fulfillment
217 of the so-called consistency condition:

$$\sum_{I=1}^{n_p} \Psi_I(\xi) \mathbf{p}(\xi_I) = \mathbf{p}(\xi) \quad (27)$$

218 or equivalently

$$\sum_{I=1}^{n_p} \Psi_I(\xi) \mathbf{p}(\xi_I - \xi) = \mathbf{p}(\mathbf{0}) \quad (28)$$

²¹⁹ Substituting Eq. (22) into (28), yields:

$$\mathbf{A}(\xi)\mathbf{c}(\xi) = \mathbf{p}(0) \Rightarrow \mathbf{c}(\xi) = \mathbf{A}^{-1}(\xi)\mathbf{p}(0) \quad (29)$$

²²⁰ where \mathbf{A} is the moment matrix:

$$\mathbf{A}(\xi) = \sum_{I=1}^{n_p} \phi(\xi_I - \xi) \mathbf{p}(\xi_I - \xi) \mathbf{p}^T(\xi_I - \xi) \quad (30)$$

²²¹ Substituting Eq. (29) back into Eq. (22), the expression of meshfree shape
²²² function can be written as:

$$\Psi_I(\xi) = \mathbf{p}^T(\xi_I - \xi) \mathbf{A}^{-1}(\xi) \mathbf{p}(0) \phi(\xi_I - \xi) \quad (31)$$

²²³ 3.2. *Reproducing kernel gradient smoothing approximation for effective stress
224 and strain*

²²⁵ In Galerkin meshfree formulation, the mid-plane of thin shell Ω is split by
²²⁶ a set of integration cells Ω_C 's, $\cup_{C=1}^{n_e} \Omega_C \approx \Omega$, as shown in Fig. 2. With the
²²⁷ inspiration of reproducing kernel smoothing framework, the Cartesian and co-
²²⁸ variant derivatives of displacement, $\mathbf{v}_{,\alpha}$ and $-\mathbf{v}_{,\alpha|\beta}$, in strains $\varepsilon_{\alpha\beta}$, $\kappa_{\alpha\beta}$ are
²²⁹ approximated by $(p-1)$ -th order polynomials in each integration cells. In inte-
²³⁰ gration cell Ω_C , the approximated derivatives and strains denoted by $\mathbf{v}_{,\alpha}^h$, $\varepsilon_{\alpha\beta}^h$
²³¹ and $-\mathbf{v}_{,\alpha|\beta}^h$, $\kappa_{\alpha\beta}^h$ can be expressed by:

$$\mathbf{v}_{,\alpha}^h(\xi) = \mathbf{q}^T(\xi) \mathbf{d}_{\alpha}^{\varepsilon}, \quad \varepsilon_{\alpha\beta}^h(\xi) = \mathbf{q}^T(\xi) \frac{1}{2} (\mathbf{a}_{\alpha} \cdot \mathbf{d}_{\beta}^{\varepsilon} + \mathbf{a}_{\beta} \cdot \mathbf{d}_{\alpha}^{\varepsilon}) \quad (32)$$

$$-\mathbf{v}_{,\alpha|\beta}^h(\xi) = \mathbf{q}^T(\xi) \mathbf{d}_{\alpha\beta}^{\kappa}, \quad \kappa_{\alpha\beta}^h(\xi) = \mathbf{q}^T(\xi) \mathbf{a}_3 \cdot \mathbf{d}_{\alpha\beta}^{\kappa} \quad (33)$$

²³² where \mathbf{q} is the linear polynomial vector and has the following form:

$$\mathbf{q} = \{1, \xi^1, \xi^2\}^T \quad (34)$$

²³⁴ and the $\mathbf{d}_{\alpha}^{\varepsilon}$, $\mathbf{d}_{\alpha\beta}^{\kappa}$ are the corresponding coefficient vector tensors. For the con-
²³⁵ ciseness, the mixed usage of tensor and vector is introduced in this study. For
²³⁶ instance, the component of coefficient tensor vector $\mathbf{d}_{\alpha I}^{\varepsilon}$, $\mathbf{d}_{\alpha}^{\varepsilon} = \{\mathbf{d}_{\alpha I}^{\varepsilon}\}$, is a three
²³⁷ dimensional tensor, $\dim \mathbf{d}_{\alpha I}^{\varepsilon} = \dim \mathbf{v}$.

²³⁸ ~~In order to meet To satisfy~~ the integration constraint of thin shell problem,
²³⁹ the approximated stresses $N^{\alpha\beta h}$, $M^{\alpha\beta h}$ ~~are assumed to be a similar form with
strains, were assumed to have a comparable form to strains, and~~ yields:

$$N^{\alpha\beta h}(\xi) = \mathbf{q}^T(\xi) \mathbf{a}^{\alpha} \cdot \mathbf{d}_N^{\beta}, \quad \mathbf{a}_{\alpha} N^{\alpha\beta h}(\xi) = \mathbf{q}^T(\xi) \mathbf{d}_N^{\beta} \quad (35)$$

$$M^{\alpha\beta h}(\xi) = \mathbf{q}^T(\xi) \mathbf{a}_3 \cdot \mathbf{d}_M^{\alpha\beta}, \quad \mathbf{a}_3 M^{\alpha\beta h}(\xi) = \mathbf{q}^T(\xi) \mathbf{d}_M^{\alpha\beta} \quad (36)$$

²⁴² substituting the approximations of Eqs. (22), (32), (33), (35), (36) into Eqs.
²⁴³ (21c), (21d) can express $\mathbf{d}_{\beta}^{\varepsilon}$ and $\mathbf{d}_{\alpha\beta}^{\kappa}$ by \mathbf{d} as:

$$\mathbf{d}_{\beta}^{\varepsilon} = \mathbf{G}^{-1} \left(\sum_{I=1}^{n_p} (\tilde{\mathbf{g}}_{\beta I} - \bar{\mathbf{g}}_{\beta I}) \mathbf{d}_I + \hat{\mathbf{g}}_{\beta} \right) \quad (37)$$

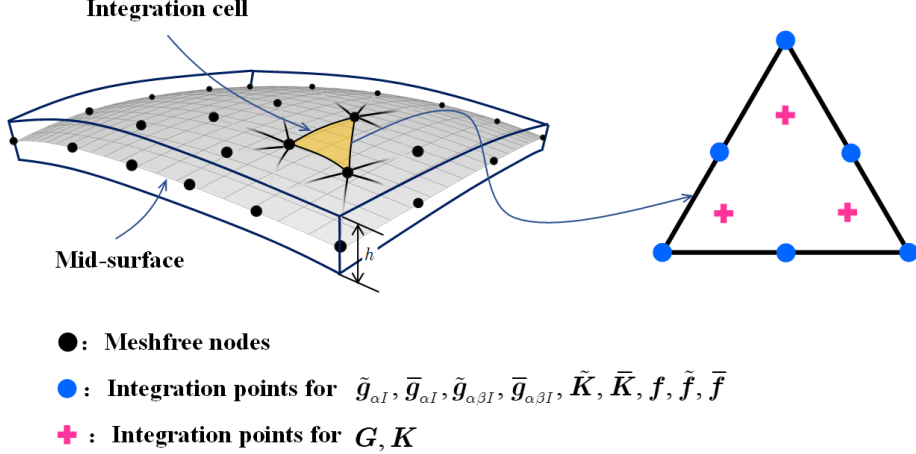


Figure 2: Integration scheme for Hu-Washizu weak form.

244

$$\mathbf{d}_{\alpha\beta}^\kappa = \mathbf{G}^{-1} \left(\sum_{I=1}^{n_p} (\tilde{\mathbf{g}}_{\alpha\beta I} - \bar{\mathbf{g}}_{\alpha\beta I}) \mathbf{d}_I + \hat{\mathbf{g}}_{\alpha\beta} \right) \quad (38)$$

245 with

$$\mathbf{G} = \int_{\Omega_C} \mathbf{q}^T \mathbf{q} d\Omega \quad (39)$$

246

$$\tilde{\mathbf{g}}_{\beta I} = \int_{\Gamma_C} \Psi_I \mathbf{q} n_\beta d\Gamma - \int_{\Omega_C} \Psi_I \mathbf{q}_{|\beta} d\Omega \quad (40a)$$

$$\bar{\mathbf{g}}_{\beta I} = \int_{\Gamma_C \cap \Gamma_v} \Psi_I \mathbf{q} n_\beta d\Gamma \quad (40b)$$

$$\hat{\mathbf{g}}_\beta = \int_{\Gamma_C \cap \Gamma_v} \mathbf{q} n_\beta \bar{\mathbf{v}} d\Gamma \quad (40c)$$

247

$$\begin{aligned} \tilde{\mathbf{g}}_{\alpha\beta I} &= \int_{\Gamma_C} \Psi_{I,\gamma} n^\gamma \mathbf{q} n_\alpha n_\beta d\Gamma - \int_{\Gamma_C} \Psi_I (\mathbf{q}_{|\beta} n_\alpha + (\mathbf{q} s_\alpha n_\beta)_{,\gamma} s^\gamma) d\Gamma \\ &\quad + [[\Psi_I \mathbf{q} s_\alpha n_\beta]]_{\mathbf{x} \in C_C} - \int_{\Omega_C} \Psi_I \mathbf{q}_{,\alpha|\beta} d\Omega \end{aligned} \quad (41a)$$

$$\begin{aligned} \bar{\mathbf{g}}_{\alpha\beta I} &= \int_{\Gamma_C \cap \Gamma_\theta} \Psi_{I,\gamma} n^\gamma \mathbf{q} n_\alpha n_\beta d\Gamma - \int_{\Gamma_C \cap \Gamma_v} \Psi_I (\mathbf{q}_{|\beta} n_\alpha + (\mathbf{q} s_\alpha n_\beta)_{,\gamma} s^\gamma) d\Gamma \\ &\quad + [[\Psi_I \mathbf{q} s_\alpha n_\beta]]_{\mathbf{x} \in C_C \cap C_v} \end{aligned} \quad (41b)$$

$$\begin{aligned} \hat{\mathbf{g}}_{\alpha\beta} &= \int_{\Gamma_C \cap \Gamma_\theta} \mathbf{q} n_\alpha n_\beta \bar{\mathbf{a}}_3 \bar{\mathbf{n}} d\Gamma - \int_{\Gamma_C \cap \Gamma_v} (\mathbf{q}_{|\beta} n_\alpha + (\mathbf{q} s_\alpha n_\beta)_{,\gamma} s^\gamma) \bar{\mathbf{v}} d\Gamma \\ &\quad + [[\mathbf{q} s_\alpha n_\beta \bar{\mathbf{v}}]]_{\mathbf{x} \in C_C \cap C_v} \end{aligned} \quad (41c)$$

²⁴⁸ where evaluations of $\mathbf{q}_{|\beta}$, $\mathbf{q}_{,\alpha|\beta}$ are ~~detail discussed~~ in Appendix A. Further
²⁴⁹ plugging Eqs. (37) and (38) back into Eqs. (32) and (33) respectively gives the
²⁵⁰ final expression of $\mathbf{v}_{,\alpha}^h$, $\varepsilon_{\alpha\beta}^h$ and $-\mathbf{v}_{,\alpha\beta}^h$, $\kappa_{\alpha\beta}^h$ as:

$$\mathbf{v}_{,\alpha}^h = \sum_{I=1}^{n_p} (\tilde{\Psi}_{I,\alpha} - \bar{\Psi}_{I,\alpha}) \mathbf{d}_I + \mathbf{q}^T \mathbf{G}^{-1} \hat{\mathbf{g}}_\alpha \quad (42a)$$

$$\begin{aligned} \varepsilon_{\alpha\beta}^h &= \sum_{I=1}^{n_p} \frac{1}{2} (\mathbf{a}_\alpha \tilde{\Psi}_{I,\beta} + \mathbf{a}_\beta \tilde{\Psi}_{I,\alpha}) \cdot \mathbf{d}_I - \sum_{I=1}^{n_p} \frac{1}{2} (\mathbf{a}_\alpha \bar{\Psi}_{I,\beta} + \mathbf{a}_\beta \bar{\Psi}_{I,\alpha}) \cdot \mathbf{d}_I \\ &\quad + \mathbf{q}^T \mathbf{G}^{-1} \frac{1}{2} (\mathbf{a}_\alpha \cdot \hat{\mathbf{g}}_\beta + \mathbf{a}_\beta \cdot \hat{\mathbf{g}}_\alpha) \\ &= \tilde{\varepsilon}_{\alpha\beta}^h - \bar{\varepsilon}_{\alpha\beta}^h + \hat{\varepsilon}_{\alpha\beta}^h \end{aligned} \quad (42b)$$

$$-\mathbf{v}_{,\alpha}^h|_\beta = \sum_{I=1}^{n_p} (\tilde{\Psi}_{I,\alpha\beta} - \bar{\Psi}_{I,\alpha\beta}) \mathbf{d}_I + \mathbf{q}^T \mathbf{G}^{-1} \hat{\mathbf{g}}_{\alpha\beta} \quad (43a)$$

$$\begin{aligned} \kappa_{\alpha\beta}^h &= \sum_{I=1}^{n_p} \tilde{\Psi}_{I,\alpha\beta} \mathbf{a}_3 \cdot \mathbf{d}_I - \sum_{I=1}^{n_p} \bar{\Psi}_{I,\alpha\beta} \mathbf{a}_3 \cdot \mathbf{d}_I + \mathbf{q}^T \mathbf{G}^{-1} \mathbf{a}_3 \cdot \hat{\mathbf{g}}_{\alpha\beta} \\ &= \tilde{\kappa}_{\alpha\beta}^h - \bar{\kappa}_{\alpha\beta}^h + \hat{\kappa}_{\alpha\beta}^h \end{aligned} \quad (43b)$$

²⁵⁴ with

$$\begin{cases} \tilde{\varepsilon}_{\alpha\beta}^h = \sum_{I=1}^{n_p} \frac{1}{2} (\mathbf{a}_\alpha \tilde{\Psi}_{I,\beta} + \mathbf{a}_\beta \tilde{\Psi}_{I,\alpha}) \cdot \mathbf{d}_I = \sum_{I=1}^{n_p} \tilde{\varepsilon}_{\alpha\beta I} \cdot \mathbf{d}_I \\ \bar{\varepsilon}_{\alpha\beta}^h = \sum_{I=1}^{n_p} \frac{1}{2} (\mathbf{a}_\alpha \bar{\Psi}_{I,\beta} + \mathbf{a}_\beta \bar{\Psi}_{I,\alpha}) \cdot \mathbf{d}_I = \sum_{I=1}^{n_p} \bar{\varepsilon}_{\alpha\beta I} \cdot \mathbf{d}_I \\ \hat{\varepsilon}_{\alpha\beta}^h = \mathbf{q}^T \mathbf{G}^{-1} \frac{1}{2} (\mathbf{a}_\alpha \cdot \hat{\mathbf{g}}_\beta + \mathbf{a}_\beta \cdot \hat{\mathbf{g}}_\alpha) \end{cases} \quad (44)$$

$$\begin{cases} \tilde{\Psi}_{I,\alpha}(\boldsymbol{\xi}) = \mathbf{q}^T(\boldsymbol{\xi}) \mathbf{G}^{-1} \tilde{\mathbf{g}}_{\alpha I} \\ \bar{\Psi}_{I,\alpha}(\boldsymbol{\xi}) = \mathbf{q}^T(\boldsymbol{\xi}) \mathbf{G}^{-1} \bar{\mathbf{g}}_{\alpha I} \\ \tilde{\varepsilon}_{\alpha\beta I} = \frac{1}{2} (\mathbf{a}_\alpha \tilde{\Psi}_{I,\beta} + \mathbf{a}_\beta \tilde{\Psi}_{I,\alpha}) \\ \bar{\varepsilon}_{\alpha\beta I} = \frac{1}{2} (\mathbf{a}_\alpha \bar{\Psi}_{I,\beta} + \mathbf{a}_\beta \bar{\Psi}_{I,\alpha}) \end{cases} \quad (45)$$

$$\begin{cases} \tilde{\kappa}_{\alpha\beta}^h = \sum_{I=1}^{n_p} \tilde{\Psi}_{I,\alpha\beta} \mathbf{a}_3 \cdot \mathbf{d}_I = \sum_{I=1}^{n_p} \tilde{\kappa}_{\alpha\beta I} \cdot \mathbf{d}_I \\ \bar{\kappa}_{\alpha\beta}^h = \sum_{I=1}^{n_p} \bar{\Psi}_{I,\alpha\beta} \mathbf{a}_3 \cdot \mathbf{d}_I = \sum_{I=1}^{n_p} \bar{\kappa}_{\alpha\beta I} \cdot \mathbf{d}_I \\ \hat{\kappa}_{\alpha\beta}^h = \mathbf{q}^T \mathbf{G}^{-1} \mathbf{a}_3 \cdot \hat{\mathbf{g}}_{\alpha\beta} \end{cases} \quad (46)$$

257

$$\begin{cases} \tilde{\Psi}_{I,\alpha\beta}(\xi) = \mathbf{q}^T(\xi) \mathbf{G}^{-1} \tilde{\mathbf{g}}_{\alpha\beta I} \\ \bar{\Psi}_{I,\alpha\beta}(\xi) = \mathbf{q}^T(\xi) \mathbf{G}^{-1} \tilde{\mathbf{g}}_{\alpha\beta I} \\ \tilde{\kappa}_{\alpha\beta I} = \tilde{\Psi}_{I,\alpha\beta} \mathbf{a}_3 \\ \bar{\kappa}_{\alpha\beta I} = \bar{\Psi}_{I,\alpha\beta} \mathbf{a}_3 \end{cases} \quad (47)$$

258 It has to be noted that, referring to reproducing kernel gradient smoothing
 259 framework [26], $\tilde{\Psi}_{I,\alpha}$, $\tilde{\Psi}_{I,\alpha\beta}$ are actually the first and second order smoothed
 260 gradients in curvilinear coordinates. ~~$\tilde{\mathbf{g}}_{\alpha I}$ and $\tilde{\mathbf{g}}_{\alpha\beta I}$~~ are If the right hand side in-
 261 tegration constraints for first and second order gradients ~~are~~ ~~$\tilde{\mathbf{g}}_{\alpha I}$ and $\tilde{\mathbf{g}}_{\alpha\beta I}$~~ ,
 262 ~~respectively~~, then this formulation can ~~meet~~ ~~satisfy~~ the variational consistency
 263 for the ~~p-th~~ ~~second~~ order polynomials. It should be known that, mentioned
 264 that in curved model, the variational consistency for non-polynomial functions,
 265 like such as trigonometric functions, should be required for the polynomial sol-
 266 lution. Even with ~~p-th order high order polynomial~~ variational consistency, the
 267 proposed formulation ~~can not~~ ~~cannot~~ exactly reproduce the solution spanned
 268 by the basis functions. However, the accuracy of reproducing kernel smoothed
 269 gradients is still better than the traditional meshfree formulation.
 270 Numerical The numerical examples in the section below will provide better
 271 evidence to prove the accuracy following section will better demonstrate the
 272 precision of the reproducing kernel smoothed gradients.

²⁷³ 4. Naturally variational enforcement for essential boundary condi-
²⁷⁴ tions

²⁷⁵ 4.1. Discrete equilibrium equations

²⁷⁶ With the approximated effective stresses and strains, the last equation of
²⁷⁷ weak form Eq. (21e) becomes:

$$-\sum_{C=1}^{n_e} \sum_{I=1}^{n_p} \delta \mathbf{d}_I \cdot \left((\tilde{\mathbf{g}}_{\alpha I}^T - \bar{\mathbf{g}}_{\alpha I}^T) \mathbf{d}_N^\alpha + (\tilde{\mathbf{g}}_{\alpha\beta I}^T - \bar{\mathbf{g}}_{\alpha\beta I}^T) \mathbf{d}_M^{\alpha\beta} \right) = -\sum_{I=1}^{n_p} \delta \underline{\mathbf{d}}_I \cdot \mathbf{f}_I \quad (48)$$

²⁷⁸ where \mathbf{f}_I 's are denote the components of the traditional force vector:

$$\mathbf{f}_I = \int_{\Gamma_t} \Psi_I \bar{\mathbf{t}} d\Gamma - \int_{\Gamma_M} \Psi_{I,\gamma} n^\gamma \bar{M}_{\mathbf{n}\mathbf{n}} d\Gamma + [[\Psi_I \mathbf{a}_3 \bar{P}]]_{\mathbf{x} \in C_P} + \int_{\Omega} \Psi_I \bar{\mathbf{b}} d\Omega \quad (49)$$

²⁷⁹ The left side of Eq. (48) can be simplified using the following steps. For clarity,
²⁸⁰ the derivation of first term in Eq. (48) taken as an example is given by:

$$\begin{aligned} \sum_{I=1}^{n_p} \delta \mathbf{d}_I \cdot \tilde{\mathbf{g}}_{\alpha I}^T \mathbf{d}_N^\alpha &= \sum_{I=1}^{n_p} \delta \mathbf{d}_I \cdot (\mathbf{G}^{-1} \tilde{\mathbf{g}}_{\alpha I})^T \mathbf{G} \mathbf{d}_N^\alpha \\ &= \int_{\Omega_C} \sum_{I=1}^{n_p} \delta \mathbf{d}_I \cdot (\mathbf{q}^T \mathbf{G}^{-1} \tilde{\mathbf{g}}_{\alpha I})^T \underline{\mathbf{q}}^T \mathbf{d}_N^\alpha d\Omega \\ &= \int_{\Omega_C} \sum_{I=1}^{n_p} \delta \mathbf{d}_I \cdot \mathbf{a}_\beta (\mathbf{q}^T \mathbf{G}^{-1} \tilde{\mathbf{g}}_{\alpha I})^T \underline{\mathbf{q}}^T N^{\alpha\beta h} d\Omega \\ &= \int_{\Omega_C} \delta \tilde{\varepsilon}_{\alpha\beta}^h N^{\alpha\beta h} d\Omega \end{aligned} \quad (50)$$

²⁸¹ following the above procedure and including the weak form of Eqs. (21a), (21b),
²⁸² the left side of Eq. (48) in Ω_C becomes:

$$\begin{aligned}
& \sum_{I=1}^{n_p} \delta \mathbf{d}_I \cdot \left((\tilde{\mathbf{g}}_{\alpha I}^T - \bar{\mathbf{g}}_{\alpha I}^T) \mathbf{d}_N^\alpha + (\tilde{\mathbf{g}}_{\alpha \beta I}^T - \bar{\mathbf{g}}_{\alpha \beta I}^T) \mathbf{d}_M^{\alpha \beta} \right) \\
& = \int_{\Omega_C} ((\delta \tilde{\varepsilon}_{\alpha \beta}^h - \delta \bar{\varepsilon}_{\alpha \beta}^h) N^{\alpha \beta h} + (\delta \tilde{\kappa}_{\alpha \beta}^h - \delta \bar{\kappa}_{\alpha \beta}^h) M^{\alpha \beta h}) d\Omega \\
& = \int_{\Omega_C} (\delta \tilde{\varepsilon}_{\alpha \beta}^h - \delta \bar{\varepsilon}_{\alpha \beta}^h) h C^{\alpha \beta \gamma \eta} \varepsilon_{\gamma \eta}^h + (\delta \tilde{\kappa}_{\alpha \beta}^h - \delta \bar{\kappa}_{\alpha \beta}^h) \frac{h^3}{12} C^{\alpha \beta \gamma \eta} \kappa_{\gamma \eta}^h \\
& = \int_{\Omega_C} \delta \tilde{\varepsilon}_{\alpha \beta}^h h C^{\alpha \beta \gamma \eta} \tilde{\varepsilon}_{\gamma \eta}^h d\Omega + \int_{\Omega_C} \delta \tilde{\kappa}_{\alpha \beta}^h \frac{h^3}{12} C^{\alpha \beta \gamma \eta} \tilde{\kappa}_{\gamma \eta}^h d\Omega \\
& - \int_{\Omega_C} \delta \bar{\varepsilon}_{\alpha \beta}^h h C^{\alpha \beta \gamma \eta} \bar{\varepsilon}_{\gamma \eta}^h d\Omega - \int_{\Omega_C} \delta \bar{\varepsilon}_{\alpha \beta}^h h C^{\alpha \beta \gamma \eta} \tilde{\varepsilon}_{\gamma \eta}^h d\Omega \\
& - \int_{\Omega_C} \delta \tilde{\kappa}_{\alpha \beta}^h \frac{h^3}{12} C^{\alpha \beta \gamma \eta} \bar{\kappa}_{\gamma \eta}^h d\Omega - \int_{\Omega_C} \delta \bar{\kappa}_{\alpha \beta}^h \frac{h^3}{12} C^{\alpha \beta \gamma \eta} \tilde{\kappa}_{\gamma \eta}^h d\Omega \\
& + \int_{\Omega_C} \delta \bar{\varepsilon}_{\alpha \beta}^h h C^{\alpha \beta \gamma \eta} \bar{\varepsilon}_{\gamma \eta}^h d\Omega + \int_{\Omega_C} \delta \bar{\kappa}_{\alpha \beta}^h \frac{h^3}{12} C^{\alpha \beta \gamma \eta} \bar{\kappa}_{\gamma \eta}^h d\Omega \\
& + \int_{\Omega_C} (\delta \tilde{\varepsilon}_{\alpha \beta}^h - \delta \bar{\varepsilon}_{\alpha \beta}^h) h C^{\alpha \beta \gamma \eta} \hat{\varepsilon}_{\gamma \eta}^h d\Omega + \int_{\Omega_C} (\delta \tilde{\kappa}_{\alpha \beta}^h - \delta \bar{\kappa}_{\alpha \beta}^h) \frac{h^3}{12} C^{\alpha \beta \gamma \eta} \hat{\kappa}_{\gamma \eta}^h d\Omega
\end{aligned} \tag{51}$$

²⁸³ ~~on~~ The complete discrete equilibrium equations can be obtained by further
²⁸⁴ substituting Eqs. (44) and (46) into above equation gives the final discrete
²⁸⁵ equilibrium equations, respectively:

$$(\mathbf{K} + \tilde{\mathbf{K}} + \bar{\mathbf{K}}) \mathbf{d} = \mathbf{f} + \tilde{\mathbf{f}} + \bar{\mathbf{f}} \tag{52}$$

²⁸⁶ where the components of stiffness matrices and force vectors in discrete equilibrium
²⁸⁷ equations can be evaluated as follows:

$$\mathbf{K}_{IJ} = \int_{\Omega} \tilde{\varepsilon}_{\alpha \beta I} h C^{\alpha \beta \gamma \eta} \tilde{\varepsilon}_{\gamma \eta J} d\Omega + \int_{\Omega} \tilde{\kappa}_{\alpha \beta I} \frac{h^3}{12} C^{\alpha \beta \gamma \eta} \tilde{\kappa}_{\alpha \beta J} d\Omega \tag{53}$$

²⁸⁸

$$\begin{aligned}
\tilde{\mathbf{K}}_{IJ} & = - \int_{\Gamma_v} (\Psi_I \tilde{\mathbf{T}}_{NJ} + \tilde{\mathbf{T}}_{NJ} \Psi_J) d\Gamma \\
& + \int_{\Gamma_\theta} (\Psi_{I,\gamma} n^\gamma \mathbf{a}_3 \tilde{\mathbf{M}}_{nnJ} + \mathbf{a}_3 \tilde{\mathbf{M}}_{nnI} \Psi_{I,\gamma} n^\gamma) d\Gamma \\
& + ([[\Psi_I \mathbf{a}_3 \tilde{\mathbf{P}}_J]] + [[\tilde{\mathbf{P}}_I \mathbf{a}_3 \Psi_J]])_{\mathbf{x} \in C_v}
\end{aligned} \tag{54a}$$

$$\tilde{\mathbf{f}}_I = - \int_{\Gamma_v} \tilde{\mathbf{T}}_{NI} \cdot \bar{\mathbf{v}} d\Gamma + \int_{\Gamma_\theta} \tilde{\mathbf{M}}_{nnI} \bar{\theta}_n d\Gamma + [[\tilde{\mathbf{P}}_I \mathbf{a}_3 \cdot \bar{\mathbf{v}}]]_{\mathbf{x} \in C_v} \tag{54b}$$

$$\bar{\mathbf{K}}_{IJ} = - \int_{\Gamma_v} \bar{\mathbf{T}}_{MI} \Psi_J d\Gamma + \int_{\Gamma_\theta} \mathbf{a}_3 \bar{\mathbf{M}}_{nnI} \Psi_{J,\gamma} n^\gamma d\Gamma + [[\bar{\mathbf{P}}_I \mathbf{a}_3 \Psi_J]]_{x \in C_v} \quad (55a)$$

$$\bar{\mathbf{f}}_I = - \int_{\Gamma_v} \bar{\mathbf{T}}_{MI} \cdot \bar{\mathbf{v}} d\Gamma + \int_{\Gamma_\theta} \bar{\mathbf{M}}_{nnI} \bar{\theta}_n d\Gamma + [[\bar{\mathbf{P}}_I \mathbf{a}_3 \cdot \bar{\mathbf{v}}]]_{x \in C_v} \quad (55b)$$

290 The detailed derivations of Eqs (53)-(55) are listed in the Appendix B. As
 291 shown in these equations, Eq. (53) is the conventional stiffness matrix evaluated
 292 by smoothed gradients $\bar{\Psi}_{I,\alpha}$, $\bar{\Psi}_{I,\alpha}|_\beta$, and the Eqs. (54) and (55) contribute for
 293 the enforcement of essential boundary. It should be mentioned noticed that,
 294 in accordance with reproducing kernel smoothed gradient framework, the in-
 295 tegration scheme of Eqs. (53-55) should be aligned with the-those used in
 296 the construction of smoothed gradients. The integration scheme used for the
 297 proposed method is shown in Fig. 2, the-in which the total number of the
blue circular integration points has been optimized from a global point of view,
aiming to reduce the computation of traditional meshfree shape functions and
its first order derivatives. In contrast, for assembly stiffness matrix \mathbf{K} , the
 301 low order Gauss integration rule is suitable to ensure the accuracy due to the
inherently variational consistency in the smoothed gradients. The detailed po-
 302 sitions and weight of integration points the integration points and the efficiency
 303 demonstration of this optimized integration scheme can be found in [33]. With a
 304 close look at [26, 33]. Examining Eqs. (54) and (55), the proposed approach for
 305 enforcing closely reveal that the structure of the suggested approach to enforce
 306 essential boundary conditions show an identical structure with traditional is
 307 identical to that of the conventional Nitsche's method, both have with both
 308 having the consistent and stabilized terms. So, the next subsection will review
 309 the. Thus, a review of Nitsche's method and compare it a comparison with the
 310 proposed method. approach will be provided in the next subsection.
 311

312 4.2. Comparison with Nitsche's method

313 The Nitsche's method for enforcing essential boundaries can be regarded as a
 314 combination of Lagrangian multiplier method and penalty method, in which the
 315 Lagrangian multiplier is represented by the approximated displacement. The

³¹⁶ corresponding total potential energy functional Π_P is given by:

$$\begin{aligned} \Pi_P(\mathbf{v}) = & \int_{\Omega} \frac{1}{2} \varepsilon_{\alpha\beta} N^{\alpha\beta} d\Omega + \int_{\Omega} \frac{1}{2} \kappa_{\alpha\beta} M^{\alpha\beta} d\Omega \\ & - \int_{\Gamma_t} \mathbf{v} \cdot \bar{\mathbf{t}} d\Gamma + \int_{\Gamma_M} \mathbf{v}_{,\gamma} n^\gamma \mathbf{a}_3 M_{\mathbf{n}\mathbf{n}} d\Gamma + (\mathbf{v} \cdot \mathbf{a}_3 P)_{\mathbf{x} \in C_P} - \int_{\Omega} \mathbf{v} \cdot \bar{\mathbf{b}} d\Omega \\ & - \underbrace{\int_{\Gamma_v} \mathbf{t} \cdot (\mathbf{v} - \bar{\mathbf{v}}) d\Gamma + \int_{\Gamma_\theta} M_{\mathbf{n}\mathbf{n}} (\theta_{\mathbf{n}} - \bar{\theta}_{\mathbf{n}}) d\Gamma + (P \mathbf{a}_3 \cdot (\mathbf{v} - \bar{\mathbf{v}}))_{\mathbf{x} \in C_v}}_{\text{consistent term}} \quad (56) \\ & + \underbrace{\sum_{i=1}^3 \frac{\alpha_{\mathbf{v}\mathbf{v}_i}}{2} \int_{\Gamma_v} (\mathbf{v} \cdot \mathbf{a}_i)^2 \mathbf{v} d\Gamma + \frac{\alpha_\theta}{2} \int_{\Gamma_\theta} \theta_{\mathbf{n}}^2 d\Gamma + \frac{\alpha_C}{2} (\mathbf{v} \cdot \mathbf{a}_3)^2 \mathbf{v}}_{\text{stabilized term}} \end{aligned}$$

³¹⁷ where the consistent term generated from the Lagrangian multiplier method
³¹⁸ contributes to enforce the essential boundary, and meet the variational consistency condition.
³¹⁹ However, the consistent term can not always ensure the coercivity of stiffness, so the penalty method is introduced to serve as a stabilized term, in which $\alpha_{\mathbf{v}i}$ is the experimental artificial parameter to enforce the displacement towards the \mathbf{a}_i direction, α_θ and α_C are parameters to enforce rotation and corner deflection, respectively. With a standard variational argument, the corresponding weak form can be stated as:

$$\begin{aligned} \delta \Pi_P(\mathbf{v}) = & \int_{\Omega} \delta \varepsilon_{\alpha\beta} N^{\alpha\beta} d\Omega + \int_{\Omega} \delta \kappa_{\alpha\beta} M^{\alpha\beta} d\Omega \\ & - \int_{\Gamma_t} \delta \mathbf{v} \cdot \bar{\mathbf{t}} d\Gamma + \int_{\Gamma_M} \delta \mathbf{v}_{,\gamma} n^\gamma \mathbf{a}_3 M_{\mathbf{n}\mathbf{n}} d\Gamma + (\delta \mathbf{v} \cdot \mathbf{a}_3 P)_{\mathbf{x} \in C_P} - \int_{\Omega} \delta \mathbf{v} \cdot \bar{\mathbf{b}} d\Omega \\ & - \int_{\Gamma_v} \delta \mathbf{v} \cdot \mathbf{t} d\Gamma + \int_{\Gamma_\theta} \delta \theta_{\mathbf{n}} M_{\mathbf{n}\mathbf{n}} d\Gamma + (\mathbf{v} \cdot \mathbf{a}_3 P)_{\mathbf{x} \in C_v} \\ & - \int_{\Gamma_v} \delta \mathbf{t} \cdot (\mathbf{v} - \bar{\mathbf{v}}) d\Gamma + \int_{\Gamma_\theta} \delta M_{\mathbf{n}\mathbf{n}} (\theta_{\mathbf{n}} - \bar{\theta}_{\mathbf{n}}) d\Gamma + (\delta P \mathbf{a}_3 \cdot (\mathbf{v} - \bar{\mathbf{v}}))_{\mathbf{x} \in C_v} \\ & + \sum_{i=1}^3 \alpha_{\mathbf{v}\mathbf{v}_i} \int_{\Gamma_v} (\delta \mathbf{v} \cdot \mathbf{a}_i)(\mathbf{a}_i \cdot \mathbf{v}) d\Gamma + \alpha_\theta \int_{\Gamma_\theta} \delta \theta_{\mathbf{n}} \theta_{\mathbf{n}} d\Gamma + \alpha_C (\delta \mathbf{v} \cdot \mathbf{a}_3 \mathbf{a}_3 \cdot \mathbf{v})_{\mathbf{x} \in C_v} \\ & = 0 \end{aligned} \quad (57)$$

³²⁵ in which α_v , α_θ and α_C represent experimental artificial parameters. Further
³²⁶ Upon further invoking the conventional reproducing kernel approximation of
³²⁷ Eq. (22) leads to the following, the subsequent discrete equilibrium equations \div
³²⁸ can be obtained:

$$\sum_{J=1}^{n_p} (\mathbf{K}_{\underline{I}\underline{J}} + \mathbf{K}^c_{\underline{I}\underline{J}} + \mathbf{K}^s_{\underline{I}\underline{J}}) \mathbf{d}_{\underline{J}} = \mathbf{f}_{\underline{I}} + \mathbf{f}^c + \mathbf{f}^s \quad (58)$$

329 where the stiffness $\mathbf{K}_{IJ} - \mathbf{K}$ is identical with Eq. (53). \mathbf{K}_{IJ}^c and \mathbf{K}_{IJ}^s \mathbf{K}^c and
 330 \mathbf{K}^s are the stiffness matrices for consistent and stabilized terms, respectively,
 331 and their components have the following form:

$$\begin{aligned}\mathbf{K}_{IJ}^c = & - \int_{\Gamma_v} (\Psi_I \mathbf{T}_{NJ} + \mathbf{T}_{\underline{N} \underline{J} \underline{N} I} \Psi_J) d\Gamma \\ & + \int_{\Gamma_\theta} (\Psi_{I,\gamma} n^\gamma \mathbf{a}_3 \mathbf{M}_{nn,I} + \mathbf{a}_3 \mathbf{M}_{nn,I} \Psi_{I,\gamma} \underline{J} \underline{\gamma} n^\gamma) d\Gamma \\ & + ([[\Psi_I \mathbf{a}_3 \mathbf{P}_J]] + [[\mathbf{P}_I \mathbf{a}_3 \Psi_J]])_{\mathbf{x} \in C_v}\end{aligned}\quad (59a)$$

$$\mathbf{f}_I^c = - \int_{\Gamma_v} \mathbf{T}_I \cdot \bar{\mathbf{v}} d\Gamma + \int_{\Gamma_\theta} \mathbf{M}_{nn,I} \bar{\mathbf{v}} d\Gamma + [[\mathbf{P}_I \mathbf{a}_3 \cdot \bar{\mathbf{v}}]]_{\mathbf{x} \in C_v} \quad (59b)$$

332

$$\mathbf{K}_{IJ}^s = \underline{\alpha_v} \underline{\alpha_v} \int_{\Gamma_v} \Psi_I \Psi_J \mathbf{1} d\Gamma + \alpha_\theta \int_{\Gamma_\theta} \Psi_{I,\eta} n^\eta \mathbf{a}_3 \mathbf{a}_3 n^\gamma \Psi_{J,\gamma} d\Gamma + \alpha_C [[\Psi_I \mathbf{a}_3 \mathbf{a}_3 \Psi_J]]_{\mathbf{x} \in C_v} \quad (60a)$$

$$\mathbf{f}_I^s = \underline{\alpha_v} \underline{\alpha_v} \int_{\Gamma_v} \Psi_I \bar{\mathbf{v}} d\Gamma + \alpha_\theta \int_{\Gamma_\theta} \Psi_{I,\eta} n^\eta \mathbf{a}_3 \bar{\mathbf{v}} d\Gamma + \alpha_C [[\Psi_I \mathbf{a}_3 \mathbf{a}_3 \cdot \bar{\mathbf{v}}]]_{\mathbf{x} \in C_v} \quad (60b)$$

333 with

$$\underline{\alpha_v} = \begin{bmatrix} \alpha_{v1} & 0 & 0 \\ 0 & \alpha_{v2} & 0 \\ 0 & 0 & \alpha_{v3} \end{bmatrix} \quad (61)$$

334 On comparing with the consistent terms of Eqs. (54) and (59), the ex-
 335 pressions were almost identical, the major difference is that the higher order
 336 derivatives of shape functions have been replaced by the smoothed gradients.
 337 Owing to the reproducing kernel framework, the construction of the smoothed
 338 gradients only concerned about the computation of traditional meshfree shape
 339 functions and their first order derivatives, which avoid the costly computation
 340 of higher order derivatives. Moreover, the stabilized terms in Eq. (60) employs
 341 the penalty method with big enough artificial parameters to ensure the coercivity
 342 of stiffness. Besides, the optimal values of these artificial parameters are
 343 proportional to the grid size of discrete model that can be represented by the
 344 support size in meshfree approximation, where $\alpha_{va} \propto s^{-1}$, $\alpha_{v3} \propto s^{-3}$, $\alpha_\theta \propto s^{-1}$,
 345 $\alpha_C \propto s^{-2}$ [31], and $s = \min\{s_{all}\}$. In contrast, the stabilized term of Eq. (55)
 346 naturally exists in its weak form, and can stabilize the result without considering
 347 any artificial parameters.

348 5. Numerical examples

349 ~~The suggested method, which uses~~ In this section, the suggested method is
 350 ~~validated through several examples using the~~ Nitsche's method, the consistent
 351 reproducing kernel gradient smoothing integration scheme (RKGSI), and the
 352 non-consistent Gauss integration scheme (GI) with penalty method, as well as
 353 the proposed Hu-Washizu formulation (HW) to enforce the necessary boundary
 354 conditions, ~~is validated in this section through several examples~~. A normalized
 355 support size of 2.5 is used for all the ~~considered~~ methods to ensure the require-
 356 ment of quadratic base meshfree approximation. To eliminate the influence of
 357 integration ~~error~~, the Gauss integration scheme uses 6 Gauss points for domain
 358 integration and 3 points for boundary integration, so as to maintain the same
 359 integration accuracy between domain and boundaries. Moreover, the number
 360 of integration points are identical between the Gauss and RKGSI schemes. The
 361 error estimates of displacement (L_2 -Error) and energy (H_e -Error) is used here:

$$L_2\text{-Error} = \frac{\sqrt{\int_{\Omega}(\mathbf{v} - \mathbf{v}^h) \cdot (\mathbf{v} - \mathbf{v}^h) d\Omega}}{\sqrt{\mathbf{v} \cdot \mathbf{v}}}$$

$$H_e\text{-Error} = \frac{\sqrt{\int_{\Omega} \left((\varepsilon_{\alpha\beta} - \varepsilon_{\alpha\beta}^h)(N^{\alpha\beta} - N^{\alpha\beta h}) + \int_{\Omega} (\kappa_{\alpha\beta} - \kappa_{\alpha\beta}^h)(M^{\alpha\beta} - M^{\alpha\beta h}) \right) d\Omega}}{\sqrt{\int_{\Omega} (\varepsilon_{\alpha\beta} N^{\alpha\beta} + \kappa_{\alpha\beta} M^{\alpha\beta}) d\Omega}}$$
(62)

362 5.1. Patch tests

363 The linear and quadratic patch tests for flat and curved thin shells are
 364 firstly studied to verify the variational consistency of the proposed method.
 365 As shown in Fig. 3, the flat and curved models are depicted by an identical
 366 parametric domain $\Omega = (0, 1) \otimes (0, 1)$, where the cylindrical coordinate sys-
 367 tem with radius $R = 1$, ~~thickness $h = 0.1$~~ is employed to describe the curved
 368 model, and the whole domain Ω is discretized by the 165 meshfree nodes. ~~The~~
 369 ~~Young's modulus and Poisson's ratio of thin shell are set to $E = 1$, $\nu = 0$.~~
 370 ~~The artificial parameters of $\alpha_v = 10^5 \times E$, $\alpha_\theta = 10^3 \times E$, $\alpha_C = 10^5 \times E$ and~~
 371 ~~$\alpha_v = 10^9 \times E$, $\alpha_\theta = 10^9 \times E$, $\alpha_C = 10^9 \times E$ were adopted in Nitsche's and penalty-~~
 372 ~~method, respectively.~~ All the boundaries are enforced as essential boundary con-
 373 ditions with the following manufactured exact solution:

$$\mathbf{v} = \begin{cases} (\xi^1 + 2\xi^2)^n \\ (3\xi^1 + 4\xi^2)^n \\ (5\xi^1 + 6\xi^2)^n \end{cases}, \quad n = \begin{cases} 1 & \text{Linear patch test} \\ 2 & \text{Quadratic patch test} \end{cases}$$
(63)

374 Table 1 lists the L_2 - and H_e -Error results of patch test with flat model, where
 375 the RKGSI scheme with variational consistent essential boundary enforcement,
 376 i.e. RKGSI-Nitsche and RKGSI-HW, can pass the linear and quadratic patch
 377 test. ~~In contrast, the RKGSI-Penalty cannot pass the patch test since the~~
 378 ~~Penalty method is unable to ensure the variational consistency.~~ Due to the

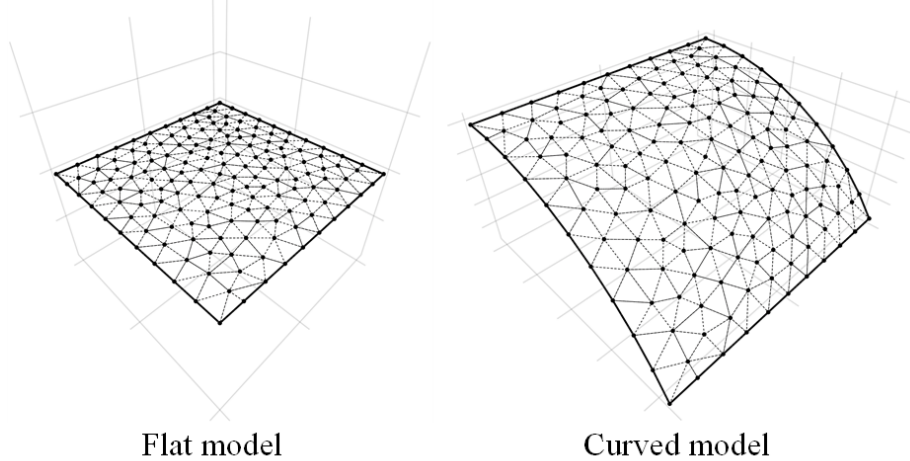


Figure 3: Meshfree discretization for patch test

loss of variational consistency condition, even with the Nitsche's method, Gauss meshfree formulations show noticeable errors. Table 2 shows the results for curved model, which indicated that all the considered methods cannot pass the patch test. This is mainly because the proposed smoothed gradient of Eqs. (35) and (36) could not exactly reproduce the non-polynomial membrane and bending stress. However
stresses. On the other hand, the RKGSI-HW and RKGSI-Nitsche methods also provide better accuracy compared to others the other approaches due to the fulfillment of first second-order variational consistency. Even only with local variational consistency, the RKGSI-Penalty obtained a better result than the traditional Gauss scheme. Meanwhile, the bending moment contours of M^{12} are listed in Fig. 4, which further verify that the proposed method provided a satisfactory result compared to the exact solution. On the other hand, the Contrarily, both the RKGSI-Penalty and the conventional Gauss meshfree formulations showed observed errors.

Table 1: Results of patch test for flat model.

	Linear patch test		Quadratic patch test	
	L_2 -Error	H_e -Error	L_2 -Error	H_e -Error
GI-Penalty	$4.45E-4$	$4.45E-04$	$1.35E-2$	$1.35E-02$
GI-Nitsche	$4.51E-4$	$4.51E-04$	$1.42E-2$	$1.42E-02$
RKGSI-Penalty	$3.64E-9$	$3.64E-09$	$6.77E-8$	$6.77E-08$
RKGSI-Nitsche	$3.31E-12$	$3.31E-12$	$1.34E-11$	$1.34E-11$
RKGSI-HR	$6.67E-13$	$6.67E-13$	$1.50E-11$	$1.50E-11$

Table 2: Results of patch test for cylindrical model.

	Linear patch test		Quadratic patch test	
	L_2 -Error	H_e -Error	L_2 -Error	H_e -Error
GI-Penalty	$3.79E-4$	$3.79E-04$	$1.30E-2$	$1.30E-02$
GI-Nitsche	$4.04E-4$	$4.04E-04$	$1.42E-2$	$1.42E-02$
RKGSI-Penalty	$1.47E-4$	$1.47E-04$	$5.39E-3$	$5.39E-03$
RKGSI-Nitsche	$2.41E-6$	$2.41E-06$	$7.37E-5$	$7.37E-05$
RKGSI-HR	$4.28E-6$	$4.28E-06$	$1.30E-4$	$1.30E-04$

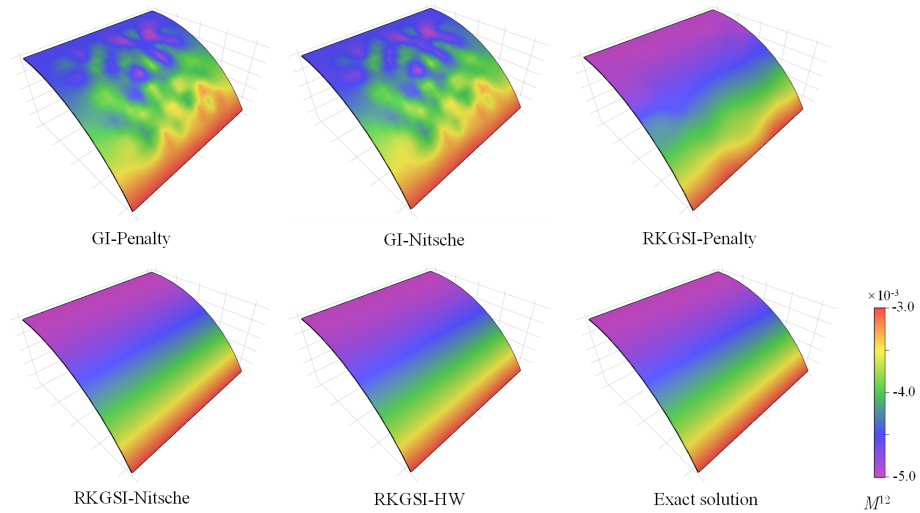


Figure 4: Contour plots of M^{12} for curved shell patch test.

393 5.2. Scordelis-Lo roof

394 This example considers the classical Scordelis-Lo roof problem, as depicted
 395 in Fig. 5. The cylindrical roof has dimensions $R = 25$, $L = 50$, $h = 0.25$,
 396 Young's modulus $E = 4.32 \times 10^8$ and Poisson's ratio $\nu = 0.0$. The entire roof
 397 is subjected to an uniform body force of $b_z = -90$, with the straight edges
 398 remaining free and the the curved edges are enforced by $v_x = v_z = 0$.

399 Due to the symmetry, only a quadrant of the model is considered for meshfree
 400 analysis, which is discretized by the 11×16 , 13×20 , 17×24 and 19×28 meshfree
 401 nodes, as listed in Fig. 6. The comparison of the displacement in z -direction at
 402 node A , v_{A3} , is used as the investigated quantity, with the reference value 0.3024
 403 given by [35] 0.3006 given by [34]. Firstly, Fig. 7 presents a sensitivity study
 404 for the artificial parameters of α_v 's, α_w 's and α_θ 's in the RKGSI meshfree
 405 formulations with Nitsche's method and penalty method. the Nitsche's- and
 406 penalty- method, where all of the parameters are scaled by the support size
 407 as, $\alpha_{v0} = s^{-1}\bar{\alpha}_v$, $\alpha_{v3} = s^{-3}\bar{\alpha}_v$ and $\alpha_\theta = s^{-1}\bar{\alpha}_\theta$. For a better comparison, the

408 result of the proposed RKGSI-HW is also listed in this figure. The results
 409 of Fig. 7 revealed, that Nitsche's method observed less artificial sensitivity.
 410 However, both the methods cannot trivially determine the optimal values of the
 411 artificial parameters. The optimal artificial parameters from Fig. 7 are adopted
 412 for the convergence study in Fig. 8. The convergence result showed that the
 413 RKGSI method get satisfactory results while the traditional Gauss methods
 414 demonstrated noticeable errors.

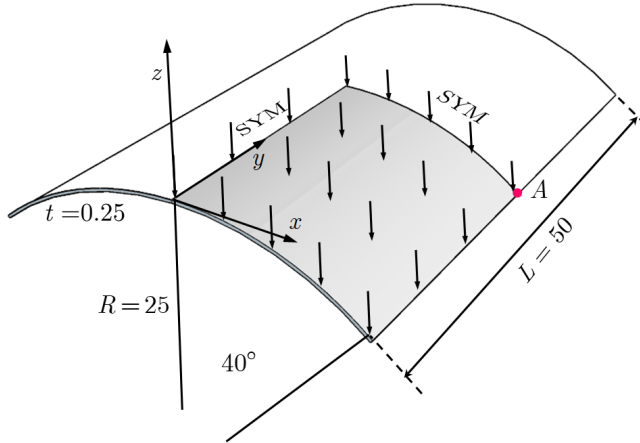


Figure 5: Description of Scordelis-Lo roof problem.

415 5.3. Pinched Hemispherical shell

416 Consider the hemispherical shell shown in Fig. 9, which is loaded at four
 417 points $P = \pm 2$ at 90° interval at its bottom. The hemispherical shell has an
 418 radius $R = 10$, thickness $h = 0.04$, Young's modulus $E = 6.825 \times 10^7$ and
 419 Poisson's ratio $\nu = 0.3$.

420 Due to symmetry, only quadrant model, where the ~~8×8, 16×16, 24×24~~ and
 421 ~~32×32 and 40×40~~ meshfree nodes have been discretized ~~was as shown in~~
 422 ~~Fig. (10)~~, were considered. The quantity under investigation for convergence
 423 is the displacement at ~~x-direction~~ on point A, $v_{A1} = 0.094$ [35].
 424 Fig. 11 displays the corresponding convergence results, indicating the RKGSI
 425 scheme performed significantly better compared to the GI meshfree formulation.
 426 Meanwhile, the efficiency comparison for this problem is also shown in Fig.
 427 12, in which the CPU time for assembly and calculation of shape functions
 428 are considered. Fig. 12(a) indicates that the RKGSI scheme observed high
 429 efficiency in assembly. This is due to the variational inconsistent Gauss meshfree
 430 formulation which require more Gaussian points to get satisfactory results. Fig.
 431 12(b) lists the CPU time spent on enforcing essential boundary conditions for
 432 the penalty method, Nitsche's method and proposed HW method. The results
 433 highlighted that the proposed HW method consumed comparable CPU time
 434 in assembly compared to Nitsche's method. However, less time was spent to

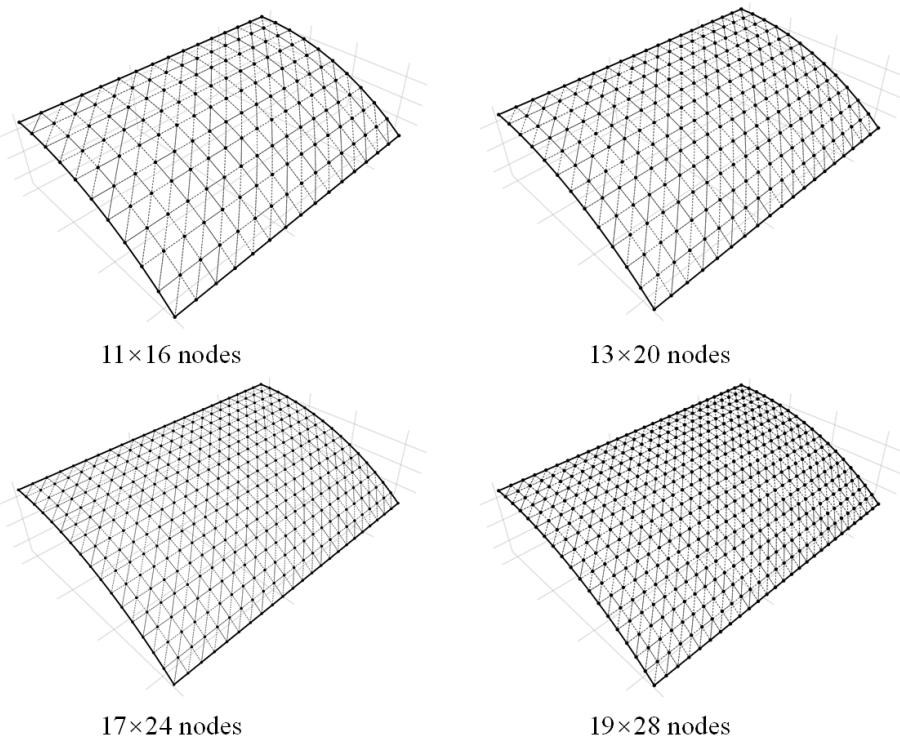
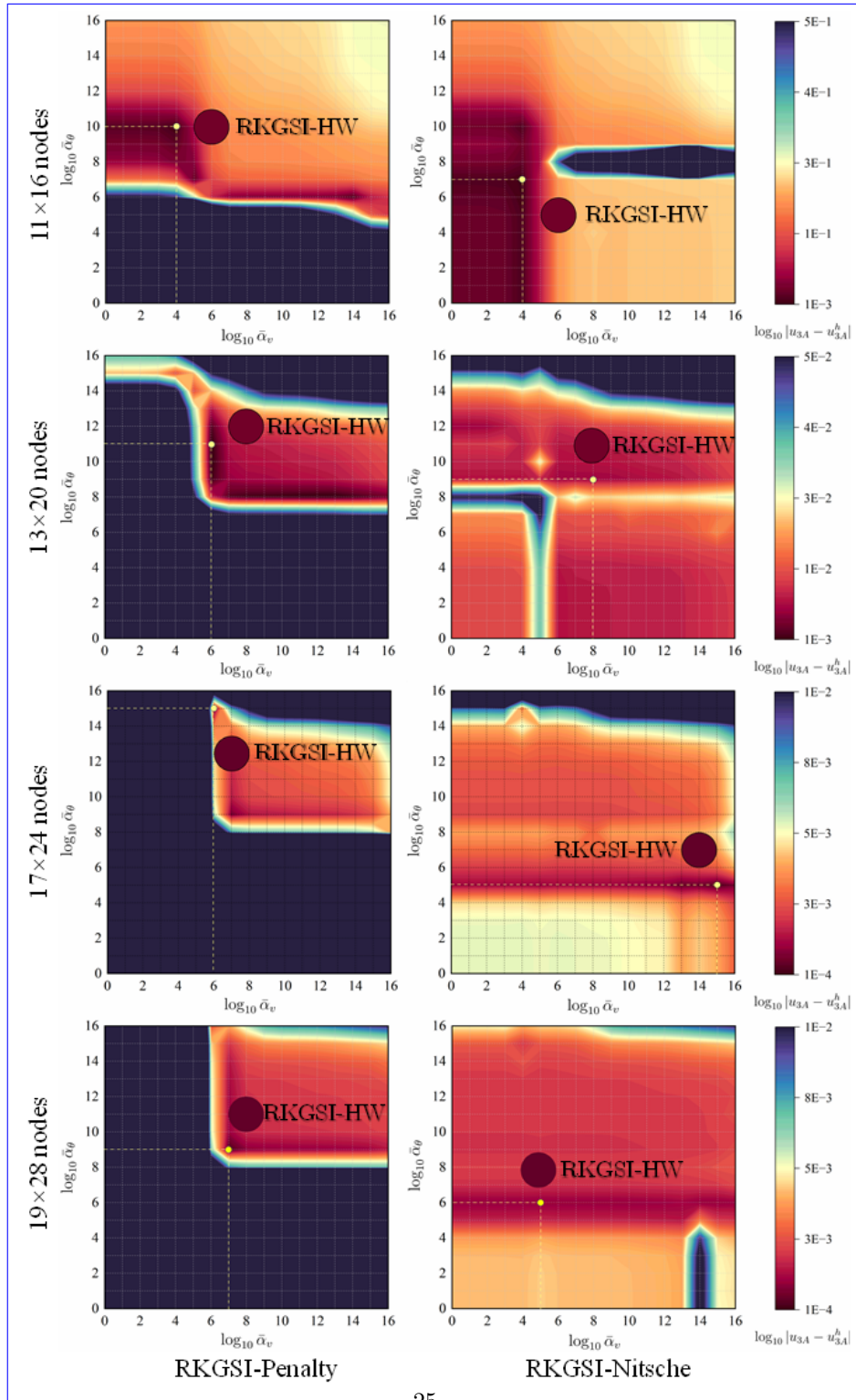


Figure 6: Meshfree discretizations for Scordelis-Lo roof problem.

⁴³⁵ calculate the shape functions. Since both the HW method and penalty method
⁴³⁶ were developed considering the shape functions first order derivatives. For this
⁴³⁷ reason, both the methods shared an almost identical time in computing the
⁴³⁸ shape functions.

Figure 7: Sensitivity comparison of α_v and α_θ for Scordelis-Lo problem.

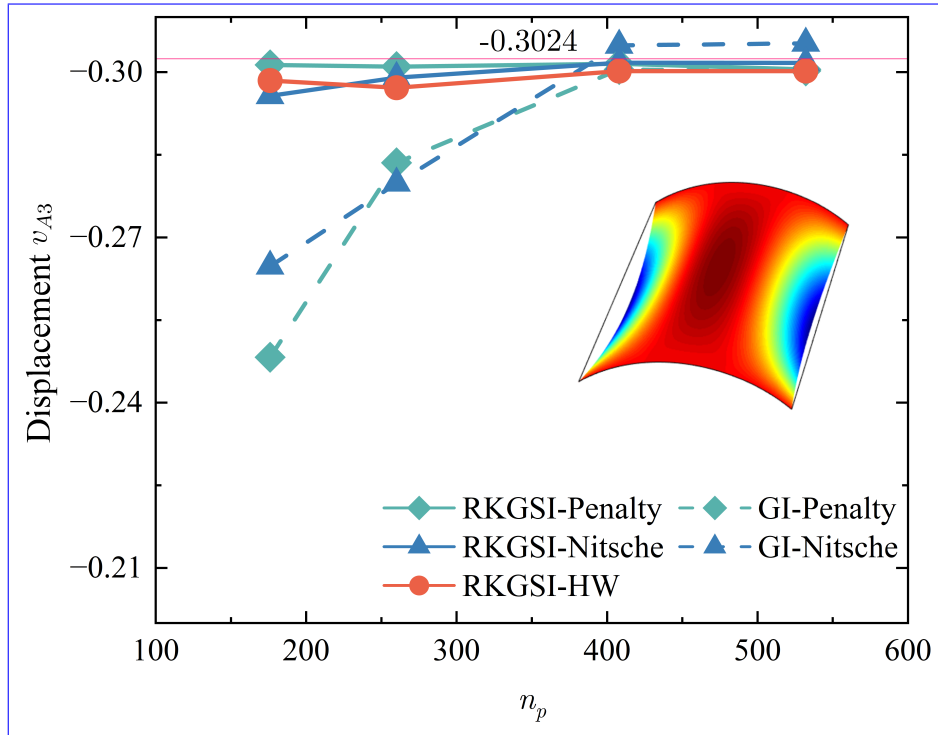


Figure 8: Displacement convergence for Scordelis-Lo roof problem.

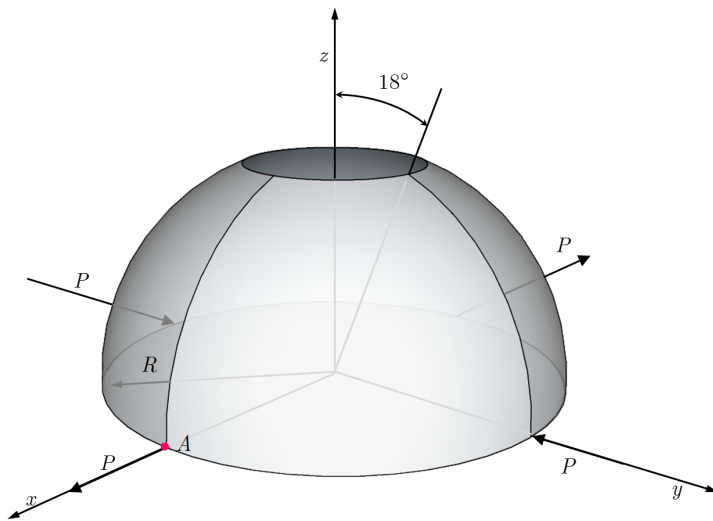


Figure 9: Description of pinched hemispherical shell problem.

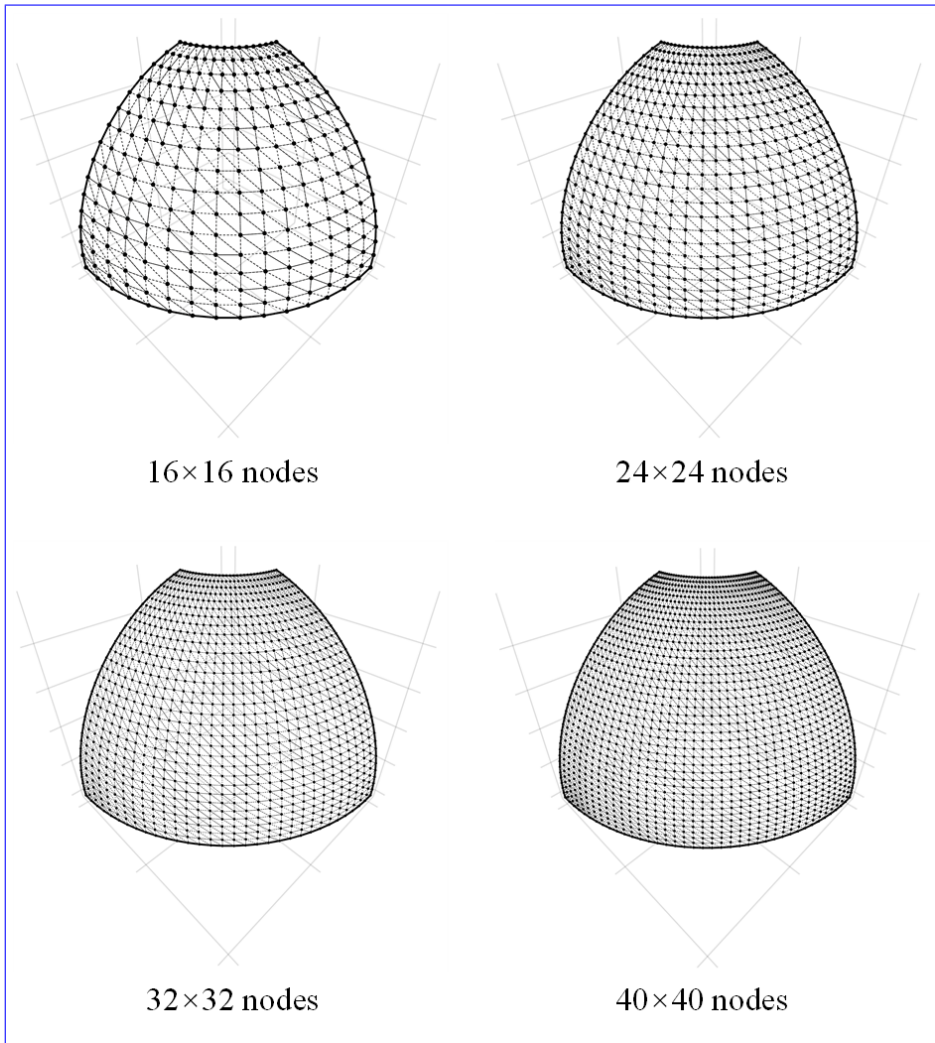


Figure 10: [Meshfree discretizations for pinched hemispherical shell problem.](#)

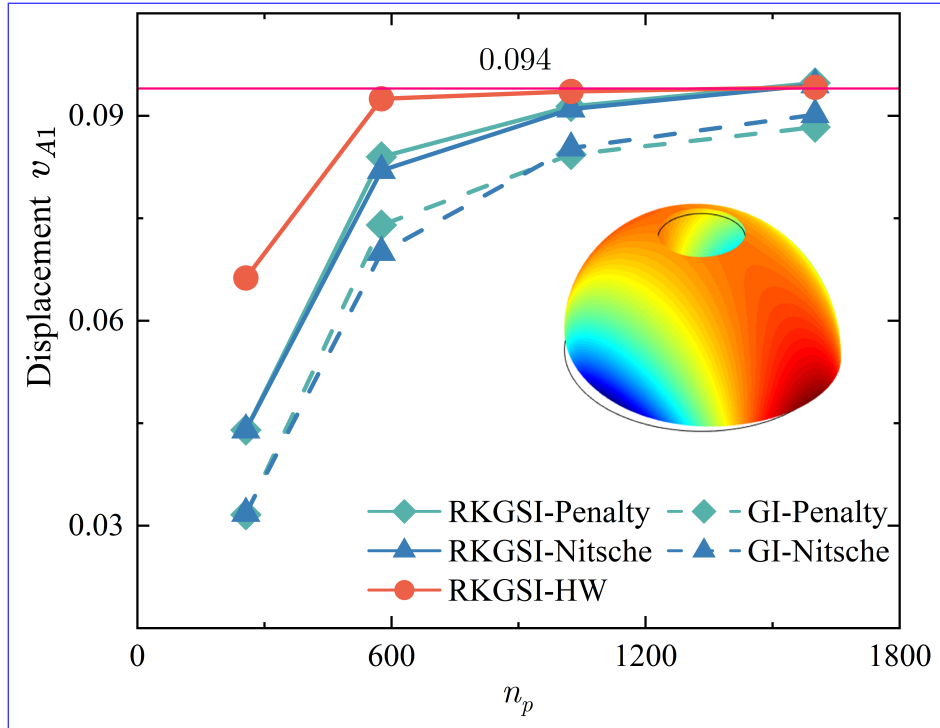


Figure 11: Displacement convergence for pinched hemispherical shell problem.

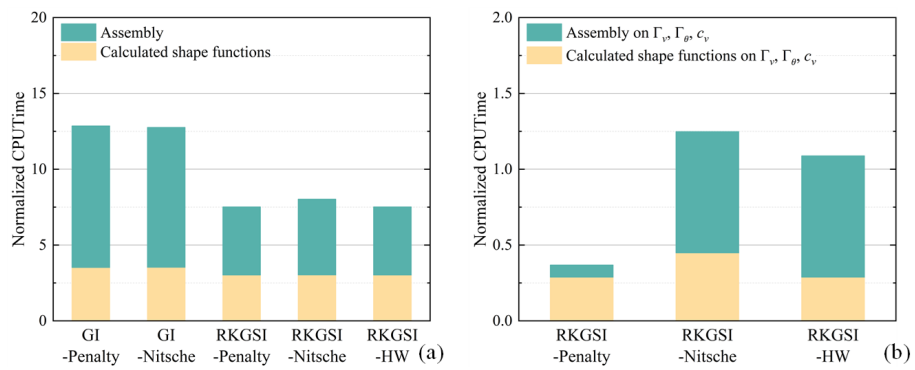


Figure 12: **efficiency** **Efficiency** comparison for pinched hemispherical shell problem: (a) Whole domain; (b) Essential boundaries

439 **6. Conclusion**

440 In this study, an efficient and quasi-consistent meshfree thin shell formu-
441 lation was presented to naturally enforce the essential boundary conditions.
442 Mixed formulation with the Hu-Washizu principle weak form is adopted, where
443 the traditional meshfree shape functions discretized the displacement, and the
444 strains and stresses were expressed by the reproducing kernel smoothed gradi-
445 ents and the covariant ~~smoothed gradients~~bases, respectively. The smoothed
446 gradient naturally embedded the first second-order integration constraints and
447 has a quasi variational consistency for the curved models in each integration cell.
448 Owing to the Hu-Washizu variational principle, the essential boundary condi-
449 tion enforcement has a similar form with the conventional Nitsche's method;
450 both have consistent and stabilized terms. The costly high order derivatives
451 in the Nitsche's consistent term have been replaced by the smoothed gradients,
452 which improved the computational speed due to the reproducing kernel gradient
453 smoothing framework. Furthermore, the stabilized term naturally existed in the
454 Hu-Washizu weak form, and the artificial parameter needed in Nitsche's stabi-
455 lized term has vanished, which can automatically maintain the coercivity for
456 the stiffness matrix. Based on general reproducing kernel gradient smoothing
457 framework, the proposed methodology can be trivially extended to high order
458 basis meshfree formulation. The numerical results demonstrated that the pro-
459 posed Hu-Washizu quasi-consistent meshfree thin shell formulation showed ex-
460 cellent accuracy, efficiency, and stability.

⁴⁶¹ **Acknowledgment**

⁴⁶² The support of this work by the National Natural Science Foundation of
⁴⁶³ China (12102138, 52350410467) and the Natural Science Foundation of Fujian
⁴⁶⁴ Province of China (2023J01108, 2022J05056) is gratefully acknowledged.

465 **Appendix A. Green's theorems for in-plane vector**

466 This Appendix discusses two kinds of Green's theorems used for the development
 467 of the proposed meshfree method. For an arbitrary vectors v^α and a
 468 scalar function f , with Green's theorem for in-plane vector, the first Green's
 469 theorem is listed as follows [31]:

$$\begin{aligned} \int_{\Omega} f_{,\alpha} v^\alpha d\Omega &= \int_{\Gamma} f v^\alpha n_\alpha d\Gamma - \int_{\Omega} f(v_{,\alpha}^\alpha + \Gamma_{\beta\alpha}^\beta v^\alpha) d\Omega \\ &= \int_{\Gamma} f v^\alpha n_\alpha d\Gamma - \int_{\Omega} f v^\alpha|_\alpha d\Omega \end{aligned} \quad (\text{A.1})$$

470 where $\Gamma_{\alpha\beta}^\gamma = \mathbf{a}_{\alpha,\beta} \cdot \mathbf{a}^\gamma$ denotes the Christoffel symbol of the second kind. $v^\alpha|_\alpha$
 471 can be represented as the in-plane covariant derivative of the vector v^α :

$$v^\alpha|_\alpha = v_{,\alpha}^\alpha + \Gamma_{\beta\alpha}^\beta v^\alpha \quad (\text{A.2})$$

472 The second Green's theorem is established with a mixed form of second
 473 order derivative. Let $A^{\alpha\beta}$ can be an arbitrary symmetric second order tensor,
 474 the Green's theorem yields [31]:

$$\begin{aligned} \int_{\Omega} f_{,\alpha}|_\beta A^{\alpha\beta} d\Omega &= \int_{\Gamma} f_{,\gamma} n^\gamma A^{\alpha\beta} n_\alpha n_\beta d\Gamma - \int_{\Gamma} f(A^{\alpha\beta} s_\alpha n_\beta)_{,\gamma} s^\gamma d\Gamma + [[f A^{\alpha\beta} s_\alpha n_\beta]]_{\mathbf{x}\in C} \\ &\quad - \int_{\Gamma} f(A_{,\beta}^{\alpha\beta} n_\alpha + \Gamma_{\alpha\beta}^\gamma A^{\alpha\beta} n_\gamma + \Gamma_{\gamma\beta}^\gamma A^{\alpha\beta} n_\alpha) d\Gamma \\ &\quad + \int_{\Omega} f \left(\begin{array}{l} \Gamma_{\alpha\beta,\gamma}^\gamma A^{\alpha\beta} + \Gamma_{\alpha\beta}^\gamma A^{\alpha\beta} + \Gamma_{\eta\gamma}^\eta \Gamma_{\alpha\beta}^\gamma A^{\alpha\beta} \\ + A_{,\alpha\beta}^{\alpha\beta} + \Gamma_{\gamma\beta,\alpha}^\gamma A^{\alpha\beta} + 2\Gamma_{\gamma\alpha}^\gamma A_{,\beta}^{\alpha\beta} + \Gamma_{\gamma\alpha}^\gamma \Gamma_{\eta\beta}^\eta A^{\alpha\beta} \end{array} \right) d\Omega \\ &= \int_{\Gamma} f_{,\gamma} n^\gamma A^{\alpha\beta} n_\alpha n_\beta d\Gamma - \int_{\Gamma} f(A^{\alpha\beta} s_\alpha n_\beta)_{,\gamma} s^\gamma d\Gamma + [[f A^{\alpha\beta} s_\alpha n_\beta]]_{\mathbf{x}\in C} \\ &\quad - \int_{\Gamma} f A^{\alpha\beta}|_\beta n_\alpha d\Gamma + \int_{\Omega} f A^{\alpha\beta}|_\alpha n_\beta d\Omega \end{aligned} \quad (\text{A.3})$$

475 with

$$A^{\alpha\beta}|_\beta = A_{,\beta}^{\alpha\beta} + \Gamma_{\beta\gamma}^\alpha A^{\beta\gamma} + \Gamma_{\gamma\beta}^\alpha A^{\alpha\beta} \quad (\text{A.4})$$

$$\begin{aligned} A^{\alpha\beta}|_{\alpha\beta} &= \Gamma_{\alpha\beta,\gamma}^\gamma A^{\alpha\beta} + \Gamma_{\alpha\beta}^\gamma A^{\alpha\beta} + \Gamma_{\eta\gamma}^\eta \Gamma_{\alpha\beta}^\gamma A^{\alpha\beta} \\ &\quad + A_{,\alpha\beta}^{\alpha\beta} + \Gamma_{\gamma\beta,\alpha}^\gamma A^{\alpha\beta} + 2\Gamma_{\gamma\alpha}^\gamma A_{,\beta}^{\alpha\beta} + \Gamma_{\gamma\alpha}^\gamma \Gamma_{\eta\beta}^\eta A^{\alpha\beta} \end{aligned} \quad (\text{A.5})$$

477 For the sake of brevity, the notion of covariant derivative is extended to a
 478 scalar function as:

$$f|_\alpha = f_{,\alpha} + \Gamma_{\beta\alpha}^\beta f \quad (\text{A.6})$$

$$f|_\beta n_\alpha = f_{,\beta} n_\alpha + \Gamma_{\alpha\beta}^\gamma f n_\gamma + \Gamma_{\gamma\beta}^\gamma f n_\alpha \quad (\text{A.7})$$

$$\begin{aligned} f|_{\alpha\beta} &= \Gamma_{\alpha\beta,\gamma}^\gamma f + \Gamma_{\alpha\beta}^\gamma f_{,\gamma} + \Gamma_{\eta\gamma}^\eta \Gamma_{\alpha\beta}^\gamma f \\ &\quad + f_{,\alpha\beta} + \Gamma_{\gamma\beta,\alpha}^\gamma f + 2\Gamma_{\gamma\alpha}^\gamma f_{,\beta} + \Gamma_{\gamma\alpha}^\gamma \Gamma_{\eta\beta}^\eta f \end{aligned} \quad (\text{A.8})$$

481 **Appendix B. Derivations for stiffness metrics and force vectors**

482 This Appendix details the derivations of stiffness matrices and force vectors
 483 in Eqs. (53)-(55), where the relationships of Eqs. (40), (41), (44) and (46) are
 484 used herein. Firstly, the membrane strain terms are considered as follows:

$$\begin{aligned}
 & \sum_{C=1}^{n_e} \int_{\Omega_C} \delta \tilde{\varepsilon}_{\alpha\beta}^h h C^{\alpha\beta\gamma\eta} \tilde{\varepsilon}_{\gamma\eta}^h d\Omega \\
 & = \sum_{C=1}^{n_e} \sum_{I,J=1}^{n_p} \delta \mathbf{d}_I \cdot \underbrace{\int_{\Omega_C} \tilde{\varepsilon}_{\alpha\beta I} h C^{\alpha\beta\gamma\eta} \mathbf{a}_\gamma \mathbf{q}^T d\Omega \mathbf{G}^{-1} \bar{\mathbf{g}}_{\eta J} \cdot \mathbf{d}_J}_{\tilde{\mathbf{g}}_I^{\eta T}} \\
 & = \sum_{C=1}^{n_e} \sum_{I,J=1}^{n_p} \delta \mathbf{d}_I \cdot \int_{\Gamma_C \cap \Gamma_v} \Psi_J \underbrace{\mathbf{q}^T \mathbf{G}^{-1} \tilde{\mathbf{g}}_I^\alpha n_\alpha}_{\tilde{\mathbf{T}}_{NI}} d\Gamma \cdot \mathbf{d}_J \\
 & = \sum_{I,J=1}^{n_p} \delta \mathbf{d}_I \cdot \int_{\Gamma_v} \tilde{\mathbf{T}}_{NI} \Psi_J d\Gamma \cdot \mathbf{d}_J
 \end{aligned} \tag{B.1}$$

485 with

$$\tilde{\mathbf{g}}_I^\alpha = \mathbf{q} \mathbf{a}_\beta h C^{\alpha\beta\gamma\eta} \tilde{\varepsilon}_{\alpha\beta\gamma\eta} \tag{B.2}$$

486

$$\tilde{\mathbf{T}}_{NI} = \mathbf{q}^T \mathbf{G}^{-1} \tilde{\mathbf{g}}_I^\alpha n_\alpha \tag{B.3}$$

487 Following this path, the bending strain terms can be reorganized by:

$$\begin{aligned}
 & \sum_{C=1}^{n_e} \int_{\Omega_C} \delta \tilde{\kappa}_{\alpha\beta}^h \frac{h^3}{12} C^{\alpha\beta\gamma\eta} \bar{\kappa}_{\gamma\eta}^h d\Omega \\
 & = \sum_{C=1}^{n_e} \sum_{I,J=1}^{n_p} \delta \mathbf{d}_I \cdot \underbrace{\int_{\Omega_C} \tilde{\kappa}_{\alpha\beta I} \frac{h^3}{12} C^{\alpha\beta\gamma\eta} \mathbf{a}_3 \mathbf{q}^T d\Omega \mathbf{G}^{-1} \bar{\mathbf{g}}_{\gamma\eta J} \cdot \mathbf{d}_J}_{\tilde{\mathbf{g}}_I^{\gamma\eta T}} \\
 & = \sum_{C=1}^{n_e} \sum_{I,J=1}^{n_p} \delta \mathbf{d}_I \cdot \left(\begin{array}{l} \int_{\Gamma_C \cap \Gamma_\theta} \underbrace{\mathbf{q}^T \mathbf{G}^{-1} \tilde{\mathbf{g}}_I^{\alpha\beta} n_\alpha n_\beta}_{\tilde{\mathbf{M}}_{nnI}} n^\gamma \Psi_{J,\gamma} d\Gamma \\ - \int_{\Gamma_C \cap \Gamma_v} \underbrace{(\mathbf{q}_{|\beta}^T \mathbf{G}^{-1} \tilde{\mathbf{g}}_I^{\alpha\beta} n_\alpha + (\mathbf{q}^T \mathbf{G}^{-1} \tilde{\mathbf{g}}_I^{\alpha\beta} s_\alpha n_\beta)_{,\gamma} s^\gamma)}_{\tilde{\mathbf{T}}_{MI}} \Psi_{J,\gamma} d\Gamma \\ + [[\underbrace{\mathbf{q}^T \mathbf{G}^{-1} \tilde{\mathbf{g}}_I^{\alpha\beta} s_\alpha n_\beta}_{\tilde{\mathbf{P}}_I \mathbf{a}_3} \Psi_J]]_{\mathbf{x} \in C_C \cap C_v} \end{array} \right) \cdot \mathbf{d}_J \\
 & = \sum_{I,J=1}^{n_p} \delta \mathbf{d}_I \cdot \left(\int_{\Gamma_\theta} \tilde{\mathbf{M}}_{nnI} n^\gamma \Psi_{J,\gamma} d\Gamma - \int_{\Gamma_v} \tilde{\mathbf{T}}_{MI} \Psi_{J,\gamma} d\Gamma + [[\tilde{\mathbf{P}}_I \Psi_J]]_{\mathbf{x} \in C_v} \right)
 \end{aligned} \tag{B.4}$$

⁴⁸⁸ with

$$\tilde{\mathbf{g}}_I^{\alpha\beta} = \int_{\Omega_C} \mathbf{q} \frac{h^3}{12} C^{\alpha\beta\gamma\eta} \mathbf{a}_3 \tilde{\kappa}_{\underline{\alpha}\underline{\beta}\underline{I}\underline{\gamma}\underline{\eta}\underline{I}} d\Omega \quad (\text{B.5})$$

⁴⁸⁹

$$\begin{cases} \tilde{M}_{nnI} = \mathbf{q}^T \mathbf{G}^{-1} \tilde{\mathbf{g}}_I^{\alpha\beta} n_\alpha n_\beta \\ \tilde{T}_{MI} = \mathbf{q}_{|\beta}^T \mathbf{G}^{-1} \tilde{\mathbf{g}}_I^{\alpha\beta} n_\alpha + (\mathbf{q}^T \mathbf{G}^{-1} \tilde{\mathbf{g}}_I^{\alpha\beta} s_\alpha n_\beta)_{,\gamma} s^\gamma \\ \tilde{P}_I = \mathbf{q}^T \mathbf{G}^{-1} \tilde{\mathbf{g}}_I^{\alpha\beta} s_\alpha n_\beta \cdot \mathbf{a}_3 \end{cases} \quad (\text{B.6})$$

490 **References**

- 491 [1] L. H. Donnell, Beams, Plates and Shells, McGraw-Hill, 1976.
- 492 [2] T. J. Hughes, The Finite Element Method: Linear Static and Dynamic
493 Finite Element Analysis, Dover Publications, Mineola, New York, 2000.
- 494 [3] T. Belytschko, Y. Y. Lu, L. Gu, Element-free Galerkin methods, International
495 Journal for Numerical Methods in Engineering 37 (1994) 229–256.
- 496 [4] W. K. Liu, S. Jun, Y. F. Zhang, Reproducing kernel particle methods,
497 International Journal for Numerical Methods in Fluids 20 (1995) 1081–
498 1106.
- 499 [5] J. S. Chen, M. Hillman, S. W. Chi, Meshfree methods: Progress made after
500 20 Years, Journal of Engineering Mechanics 143 (2017) 04017001.
- 501 [6] P. Krysl, T. Belytschko, Analysis of thin shells by the Element-Free
502 Galerkin method, International Journal of Solids and Structures 33 (1996)
503 3057–3080.
- 504 [7] G. R. Liu, Meshfree Methods: Moving Beyond the Finite Element Method,
505 Second Edition, Crc Press, 2009.
- 506 [8] X. Zhang, K. Z. Song, M. W. Lu, X. Liu, Meshless methods based on
507 collocation with radial basis functions, Computational Mechanics 26 (2000)
508 333–343.
- 509 [9] D. Millán, A. Rosolen, M. Arroyo, Thin shell analysis from scattered points
510 with maximum-entropy approximants, International Journal for Numerical
511 Methods in Engineering 85 (2011) 723–751.
- 512 [10] L. Wang, M. Hu, Z. Zhong, F. Yang, Stabilized Lagrange Interpolation
513 Collocation Method: A meshfree method incorporating the advantages of
514 finite element method, Computer Methods in Applied Mechanics and
515 Engineering 404 (2023) 115780.
- 516 [11] P. Suchde, T. Jacquemin, O. Davydov, Point Cloud Generation for Mesh-
517 free Methods: An Overview, Archives of Computational Methods in Engi-
518 neering 30 (2022) 889–915.
- 519 [12] L. Deng, D. Wang, An accuracy analysis framework for meshfree collocation
520 methods with particular emphasis on boundary effects, Computer Methods
521 in Applied Mechanics and Engineering 404 (2023) 115782.
- 522 [13] J. Wang, M. Hillman, Upwind reproducing kernel collocation method for
523 convection-dominated problems, Computer Methods in Applied Mechanics
524 and Engineering 420 (2024) 116711.

- 525 [14] S. Fernández-Méndez, A. Huerta, Imposing essential boundary conditions
 526 in mesh-free methods, Computer Methods in Applied Mechanics and En-
 527 gineering 193 (2004) 1257–1275.
- 528 [15] X. Li, Error estimates for the moving least-square approximation and the
 529 element-free Galerkin method in n-dimensional spaces, Applied Numerical
 530 Mathematics 99 (2016) 77–97.
- 531 [16] J. Wu, D. Wang, An accuracy analysis of Galerkin meshfree methods ac-
 532 counting for numerical integration, Computer Methods in Applied Mechan-
 533 ics and Engineering 375 (2021) 113631.
- 534 [17] J. S. Chen, H. P. Wang, New boundary condition treatments in meshfree
 535 computation of contact problems, Computer Methods in Applied Mechan-
 536 ics and Engineering 187 (2000) 441–468.
- 537 [18] D. Liu, Y. M. Cheng, The interpolating element-free Galerkin (IEFG)
 538 method for three-dimensional potential problems, Engineering Analysis
 539 with Boundary Elements 108 (2019) 115–123.
- 540 [19] V. Ivannikov, C. Tiago, P. M. Pimenta, On the boundary conditions of the
 541 geometrically nonlinear Kirchhoff–Love shell theory, International Journal
 542 of Solids and Structures 51 (2014) 3101–3112.
- 543 [20] Y. Y. Lu, T. Belytschko, L. Gu, A new implementation of the element free
 544 Galerkin method, Computer Methods in Applied Mechanics and Engineer-
 545 ing 113 (1994) 397–414.
- 546 [21] T. Zhu, S. N. Atluri, A modified collocation method and a penalty formu-
 547 lation for enforcing the essential boundary conditions in the element free
 548 Galerkin method, Computational Mechanics 21 (1998) 211–222.
- 549 [22] S. Skatulla, C. Sansour, Essential boundary conditions in meshfree methods
 550 via a modified variational principle: Applications to shell computations,
 551 Computer Assisted Mechanics and Engineering Sciences 15 (2008) 123–142.
- 552 [23] J. S. Chen, C. T. Wu, S. Yoon, Y. You, A stabilized conforming nodal
 553 integration for Galerkin mesh-free methods, International Journal for Nu-
 554 matical Methods in Engineering 50 (2001) 435–466.
- 555 [24] J. S. Chen, M. Hillman, M. Rüter, An arbitrary order variationally consis-
 556 tent integration for Galerkin meshfree methods, International Journal for
 557 Numerical Methods in Engineering 95 (2013) 387–418.
- 558 [25] Q. Duan, X. Li, H. Zhang, T. Belytschko, Second-order accurate derivatives
 559 and integration schemes for meshfree methods, International Journal for
 560 Numerical Methods in Engineering 92 (2012) 399–424.

- 561 [26] D. Wang, J. Wu, An inherently consistent reproducing kernel gradient
 562 smoothing framework toward efficient Galerkin meshfree formulation with
 563 explicit quadrature, Computer Methods in Applied Mechanics and Engi-
 564 neering 349 (2019) 628–672.
- 565 [27] J. Wang, X. Ren, A consistent projection integration for Galerkin meshfree
 566 methods, Computer Methods in Applied Mechanics and Engineering 414
 567 (2023) 116143.
- 568 [28] J. Wu, X. Wu, Y. Zhao, D. Wang, A consistent and efficient method for
 569 imposing meshfree essential boundary conditions via hellinger-reissner vari-
 570 ational principle., Chinese Journal of Theoretical and Applied Mechanics
 571 54 (2022) 3283–3296.
- 572 [29] J. Wu, X. Wu, Y. Zhao, D. Wang, A rotation-free Hellinger-Reissner mesh-
 573 free thin plate formulation naturally accommodating essential boundary
 574 conditions, Engineering Analysis with Boundary Elements 154 (2023) 122–
 575 140.
- 576 [30] H. Dah-wei, A method for establishing generalized variational principle,
 577 Applied Mathematics and Mechanics 6 (1985) 501–509.
- 578 [31] J. Benzaken, J. A. Evans, S. F. McCormick, R. Tamstorf, Nitsche's method
 579 for linear Kirchhoff–Love shells: Formulation, error analysis, and verifica-
 580 tion, Computer Methods in Applied Mechanics and Engineering 374 (2021)
 581 113544.
- 582 [32] H. Dah-wei, A method for establishing generalized variational principle,
 583 Applied Mathematics and Mechanics 6 (1985) 501–509.
- 584 [33] H. Du, J. Wu, D. Wang, J. Chen, A unified reproducing kernel gradient
 585 smoothing Galerkin meshfree approach to strain gradient elasticity, Com-
 586 putational Mechanics 70 (2022) 73–100.
- 587 [34] J. Kiendl, K. U. Bletzinger, J. Linhard, R. Wüchner, Isogeometric shell
 588 analysis with Kirchhoff–Love elements, Computer Methods in Applied
 589 Mechanics and Engineering 198 (2009) 3902–3914.
- 590 [35] R. H. MacNeal, R. L. Harder, A proposed standard set of problems to test
 591 finite element accuracy, Finite Elements in Analysis and Design 1 (1985)
 592 3–20.